Article

Developmental Cell

Drosophila HNF4 Directs a Switch in Lipid Metabolism that Supports the Transition to Adulthood

Graphical Abstract

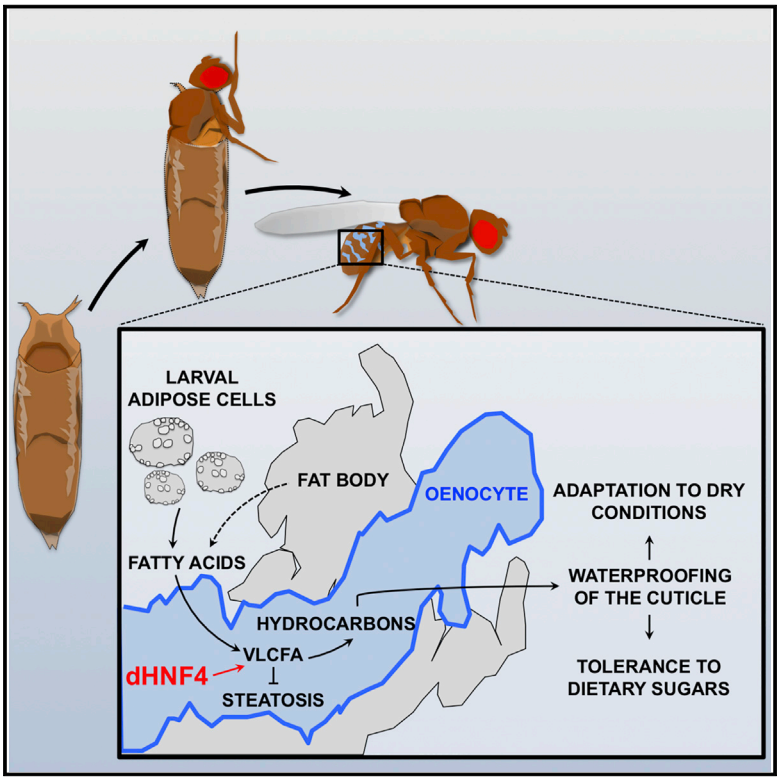

Authors

Gilles Storelli, Hyuck-Jin Nam, Judith Simcox, Claudio J. Villanueva, Carl S. Thummel

Correspondence

gstorelli@genetics.utah.edu (G.S.), carl.thummel@genetics.utah.edu (C.S.T.)

In Brief

Storelli et al. show that the *Drosophila* HNF4 nuclear receptor couples lipid metabolism with development to meet the needs of adult life. *Drosophila* HNF4 directs the rapid conversion of lipid stores into waterproofing hydrocarbons at the onset of adulthood, allowing the animal to adapt to dry conditions and dietary sugars.

Highlights

- Lipid stores are consumed rapidly after *Drosophila* transitions into adulthood
- *Drosophila* HNF4 directs fatty acid conversion to VLCFA and hydrophobic hydrocarbons
- VLCFA/hydrocarbon synthesis ensures adaptation to dry conditions and dietary sugars
- The role for HNF4 in regulating VLCFA synthesis is conserved between flies and mice

Storelli et al., 2019, Developmental Cell *48*, 200–214
January 28, 2019
https://doi.org/10.1016/j.devcel.2018.11.030

CellPress

CellPress

Developmental Cell
Article

Drosophila HNF4 Directs a Switch in Lipid Metabolism that Supports the Transition to Adulthood

Gilles Storelli,[1,*] Hyuck-Jin Nam,[1] Judith Simcox,[2] Claudio J. Villanueva,[2] and Carl S. Thummel[1,3,*]
[1]Department of Human Genetics, University of Utah School of Medicine, Salt Lake City, UT 84112-5330, USA
[2]Department of Biochemistry, University of Utah School of Medicine, Salt Lake City, UT 84112, USA
[3]Lead Contact
*Correspondence: gstorelli@genetics.utah.edu (G.S.), carl.thummel@genetics.utah.edu (C.S.T.)
https://doi.org/10.1016/j.devcel.2018.11.030

SUMMARY

Animals must adjust their metabolism as they progress through development in order to meet the needs of each stage in the life cycle. Here, we show that the dHNF4 nuclear receptor acts at the onset of *Drosophila* adulthood to direct an essential switch in lipid metabolism. Lipid stores are consumed shortly after metamorphosis but contribute little to energy metabolism. Rather, *dHNF4* directs their conversion to very long chain fatty acids and hydrocarbons, which waterproof the animal to preserve fluid homeostasis. Similarly, *HNF4α* is required in mouse hepatocytes for the expression of fatty acid elongases that contribute to a waterproof epidermis, suggesting that this pathway is conserved through evolution. This developmental switch in *Drosophila* lipid metabolism promotes lifespan and desiccation resistance in adults and suppresses hallmarks of diabetes, including elevated glucose levels and intolerance to dietary sugars. These studies establish dHNF4 as a regulator of the adult metabolic state.

INTRODUCTION

All organisms undergo a series of distinct biological programs as they advance through their life cycle. Changes in nutrition and systemic physiology must be coupled with these transitions in order to meet the specific metabolic needs of each stage in development (Li and Tennessen, 2017; Miyazawa and Aulehla, 2018). For example, the mammalian heart undergoes a switch from using glucose as an energy source during fetal stages to fatty acids after birth, as this organ increases oxidative energy metabolism (Lehman and Kelly, 2002). In *Drosophila*, a mid-embryonic transcriptional switch establishes an aerobic glycolytic metabolic state that supports larval growth (Tennessen et al., 2011). Stage-specific metabolic and physiological states may also render organisms more susceptible to nutritional stress, such as during puberty in humans (Catalano, 2010; Kelsey and Zeitler, 2016), and metabolic perturbations can feedback on developmental progression. For example, it is well known that childhood obesity alters the timing of sexual maturation (Burt Solorzano and McCartney, 2010). Moreover, disease can reverse developmental changes in physiological state, demonstrating the importance of understanding the links between development and metabolism for potential therapeutic applications (Lehman and Kelly, 2002).

Hepatocyte Nuclear Factor 4α (HNF4α, NR2A1) is a member of the nuclear receptor superfamily of ligand-regulated transcription factors. It binds long-chain fatty acids (LCFAs) and acts as a transcriptional activator, although the role of the ligand in receptor activation remains unclear (Duda et al., 2004; Wisely et al., 2002; Yuan et al., 2009). HNF4α is expressed in the intestine, liver, kidneys, and pancreas and is required for early embryonic development in mice (Chen et al., 1994; Li et al., 2000). Loss of *HNF4α* in the liver leads to hepatic lipid accumulation (steatosis) and to systemic physiological defects, including reduced levels of plasma lipid, defects in hepatic acylcarnitine production in response to cold stimulation, progressive weight loss, and a shortened lifespan (Hayhurst et al., 2001; Simcox et al., 2017). This is accompanied by changes in the expression of genes involved in lipid metabolism, suggesting that this factor plays an important role in maintaining lipid homeostasis (Hayhurst et al., 2001; Simcox et al., 2017; Yin et al., 2011). Similar phenotypes are seen in *C. elegans* and *Drosophila* mutants for homologs of *HNF4α*, suggesting that these functions are conserved through evolution (Palanker et al., 2009; Van Gilst et al., 2005). Human *HNF4α* loss-of-function mutations are also responsible for an autosomal dominant form of diabetes called Maturity Onset Diabetes of the Young 1 (MODY1) (Yamagata et al., 1996). Taken together, these observations suggest that HNF4α plays tissue-specific roles in coordinating glucose and lipid metabolism during development.

The basic mechanisms of metabolic control and intertissue communication are conserved between invertebrates and vertebrates, allowing functions discovered in the fruit fly *Drosophila* to be directly applied to our understanding of mammalian physiology and human disease (Musselman and Kühnlein, 2018; Owusu-Ansah and Perrimon, 2014; Teleman et al., 2012). The *Drosophila* genome encodes a single HNF4α ortholog called *Drosophila* HNF4 (dHNF4) that is widely expressed in the animal (Palanker et al., 2009; Zhong et al., 1993). *dHNF4* mutants progress normally through embryogenesis, larval stages, and metamorphosis. However, most animals die upon emergence from their pupal case, and the remaining escapers succumb within

the first days of adulthood (Barry and Thummel, 2016; Palanker et al., 2009). Interestingly, this early adult lethality can be partly rescued if *dHNF4* mutants are reared on a low-sugar diet (Barry and Thummel, 2016). This study also demonstrated a role for *dHNF4* in maintaining glucose homeostasis and mitochondrial function in adults. In spite of these advances, however, the metabolic basis for the adult-onset lethality and sugar toxicity in *dHNF4* mutants remains unknown.

Here, we show that specialized lipid-metabolizing cells called oenocytes become steatotic after the emergence of *dHNF4* mutant adults. This lipid accumulation progresses independently of feeding and parallels the developmental clearance of larval adipose cells that occurs during the first days of adult life (Aguila et al., 2007). Improper lipid metabolism in oenocytes does not compromise the starvation response of newly emerged *dHNF4* mutants, indicating that the fate of these lipid stores is not for energy production. Rather, oenocytes are the primary site for the production of very long chain fatty acids (VLCFA) and VLCFA-derived hydrocarbons, which are secreted and transported through the epidermis and the overlaying cuticle to act as waterproofing agents and pheromones (Makki et al., 2014; Wicker-Thomas et al., 2015; Wigglesworth, 1988). We show that *dHNF4* supports the transcriptional induction of genes involved in VLCFA and hydrocarbon synthesis shortly after adult emergence and is required in oenocytes to suppress developmental steatosis and maintain resistance to dehydration. These roles appear to be conserved through evolution since *HNF4α* is required in mouse hepatocytes for the proper expression of genes encoding fatty acid elongases, which are required to suppress hepatic steatosis and allow the survival of newborn pups in a dry environment (Aldahmesh et al., 2011; Sassa et al., 2013; Westerberg et al., 2004). Finally, we demonstrate that *dHNF4* acts through hydrocarbon production in oenocytes to preserve glucose homeostasis and suppress dietary sugar toxicity. Taken together, our work demonstrates an essential role for dHNF4 in coupling metabolism with developmental progression by directing the rapid conversion of free fatty acids into VLCFAs and hydrocarbons at the onset of adult life.

RESULTS

dHNF4 Mutants Are Short-Lived, Sensitive to Dietary Sugar, and Hyperlipidemic

All genetic studies used a transheterozygous combination of *dHNF4* null alleles (w^-; $dHNF4^{\Delta 17}/dHNF4^{433}$, referred to as *dHNF4* mutants) and genetically matched controls that are transheterozygous for precise excisions of the *EP2449* and *KG08976* P elements (referred to as controls), as described previously (Palanker et al., 2009). To investigate the physiological defects in *dHNF4* mutant adults, we reared animals during larval stages on a yeast diet devoid of sugar (0% sugar) and switched them to a 0% or a 15% sugar diet after adult emergence (Figure 1A). *dHNF4* mutant adults are short-lived compared to controls regardless of their diet. Consistent with earlier reports, adult-specific exposure to dietary carbohydrates further reduces their lifespan (Figure 1A) (Barry and Thummel, 2016). The overall short lifespan of *dHNF4* mutants and their sensitivity to dietary sugar suggests that they suffer from metabolic defects. Consistent with this, *dHNF4* mutants have low glucose and glycogen levels at 1 week of age on a sugar-free diet, and slightly lower glycogen and markedly elevated glucose levels when switched to a 15% sugar diet at emergence (Figures 1B and 1C). In contrast, 1-week-old *dHNF4* mutants are hyperlipidemic on both diets (Figures 1B and 1C). These results led to the hypothesis that defects in lipid homeostasis contribute to the short lifespan in *dHNF4* mutant adults on both the 0% and 15% sugar diets.

dHNF4 Suppresses Adult-Onset Hyperlipidemia

In order to examine lipid metabolism in more detail, we measured triglyceride (TAG) levels in staged control and *dHNF4* mutants that were either kept on the sugar-free diet or transferred to a 15% sugar diet at emergence. On the sugar-free diet, controls lose TAG during early adulthood and then recover their stored lipids between days 3 and 7 (Figure 2A). This trend is also observed in controls shifted to the 15% sugar diet at emergence, although the overall changes are reduced (Figure 2B). The early drop in TAG is consistent with the developmental clearance of lipid-containing larval adipose cells, which occurs during the first 2 days of adulthood (Aguila et al., 2007), followed by a recovery of stored lipids due to dietary uptake and *de novo* lipogenesis. Interestingly, *dHNF4* mutants begin their adult life with normal levels of TAG, demonstrating that the defects in lipid homeostasis develop after emergence (Figures 2A and 2B). They then display either a drop and recovery in TAG levels on the sugar-free diet, or a steady increase in TAG on the 15% sugar diet, with a gradual onset of hyperlipidemia on both diets. Taken together, these observations indicate that *dHNF4* is required to suppress excess lipid accumulation in newly emerged adults.

Early adulthood is characterized by the clearance of lipid-containing larval adipose cells (Aguila et al., 2007), and our previous work demonstrated that *dHNF4* regulates lipid catabolism (Palanker et al., 2009). Thus, the progressive hyperlipidemia in *dHNF4* mutants could be explained, at least in part, by reduced clearance of lipid stores. To test this, we analyzed TAG consumption in control and *dHNF4* mutants starved after emergence. We transferred newly emerged flies to empty vials sealed with a dense-weave cellulose acetate stopper saturated with water. Remarkably, under these hydrated conditions, control flies survive starvation for up to 10-fold longer than has been reported in the literature (Figure 2C; Aguila et al., 2007; Chatterjee et al., 2014). This suggests that current starvation protocols shorten lifespan by limiting their access to water. Similar results are seen when other control fly lines are subjected to starvation with constant access to hydration, although there are strain-dependent differences in lifespan (Figure S1A). Unexpectedly, *dHNF4* mutant adults are resistant to starvation compared to controls, contrary to what has been shown in larvae (Figure 2C; Palanker et al., 2009). In addition, stored lipids appear to play little role in supporting young adult survival under starvation conditions. In starved controls, TAG is cleared after 3 days even though these animals survive for several weeks (Figures 2C and 2D). In contrast, TAG is incompletely cleared in starved *dHNF4* mutants and remains stable between days 3 and 7 (Figure 2D). Thus, *dHNF4* is required for lipid catabolism, but stored fat is not limiting for the survival of young adults upon starvation.

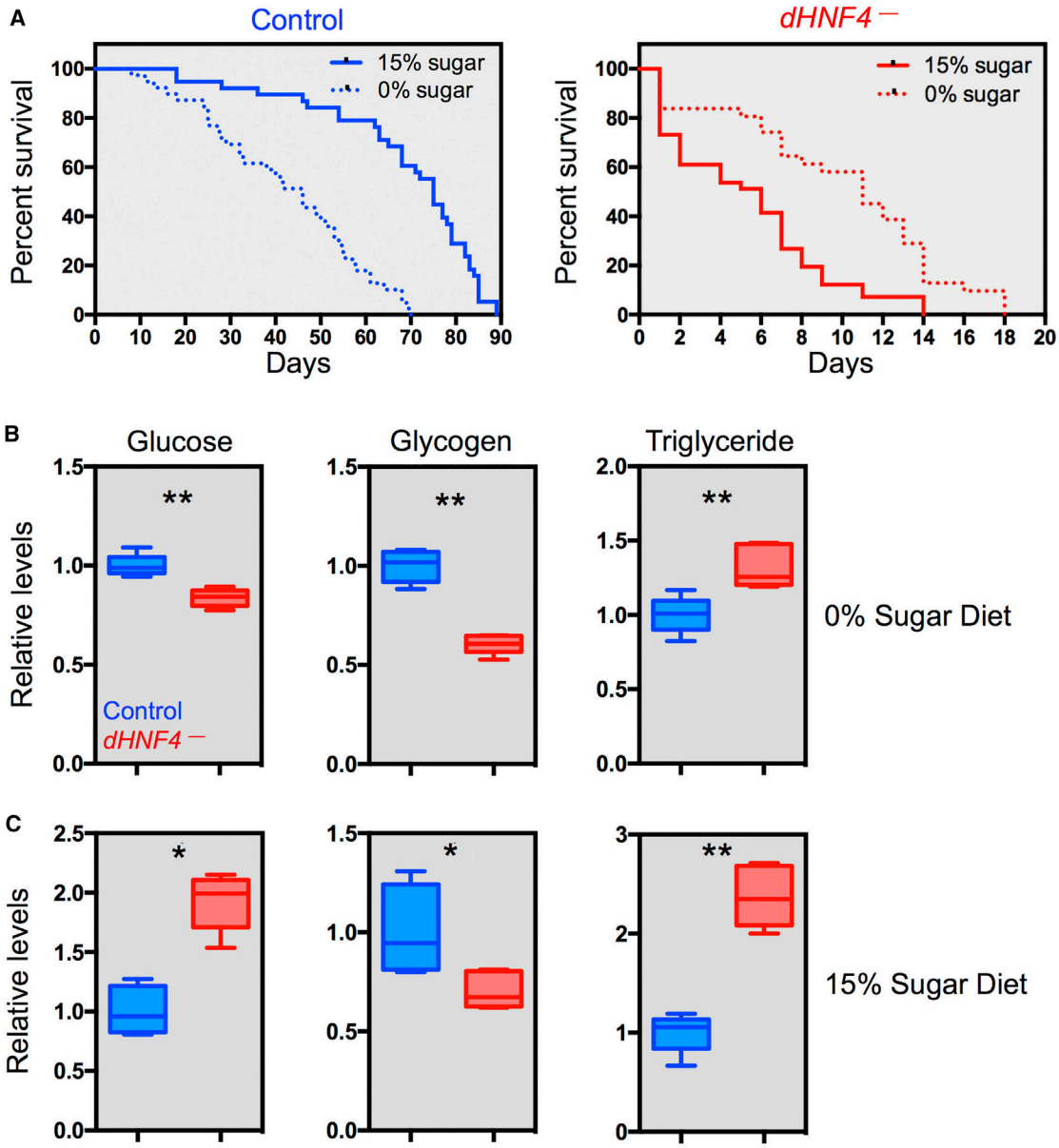

Figure 1. *dHNF4* Mutants Display a Reduced Lifespan, Sensitivity to Dietary Carbohydrates, and Defects in Metabolic Homeostasis

(A) Lifespan was scored for controls (blue) and *dHNF4* mutants (red) reared on a 0% sugar diet as larvae and transferred to a 0% (dotted line) or a 15% (solid line) sugar diet after adult emergence. Control median lifespan—0% sugar diet: 46 days (n = 46); 15% sugar diet: 75 days (n = 38); $p < 0.0001$. *dHNF4* mutant median lifespan—0% sugar diet: 11 days (n = 31); 15% sugar diet: 6 days (n = 41); $p < 0.0001$.

(B and C) Glucose, glycogen, and triglyceride levels were measured in 7-day-old control and *dHNF4* mutants reared on a 0% sugar diet (B) or a 15% sugar diet (C) after emergence. Metabolite levels are normalized to total protein and presented relative to the amount in control animals.

Analysis of other key metabolites revealed that protein levels decline by about 25% during the first week of starvation, while glucose and glycogen levels drop during the first days of starvation and then partially recover to maintain homeostasis in controls (Figures S1B–S1D). These results suggest that unlike mammals that depend on lipid-derived ketogenesis to survive starvation, fruit flies depend primarily on amino acids to support gluconeogenesis and survival (Cahill, 2006). *dHNF4* mutants emerge with less protein, glucose, and glycogen, but these metabolites follow similar trends as controls and normalize by day 7 (Figures S1B–S1D). The relatively normal use of protein and carbohydrates in starved *dHNF4* mutants likely explains the ability of these animals to persist under starvation conditions and highlights the central role of *dHNF4* in maintaining lipid homeostasis.

dHNF4 Suppresses Developmental Steatosis in Oenocytes

We examined the lipid stores of young adults to identify the tissue(s) contributing to hyperlipidemia in *dHNF4* mutants. The larval adipose cells that are free-floating in the hemolymph of

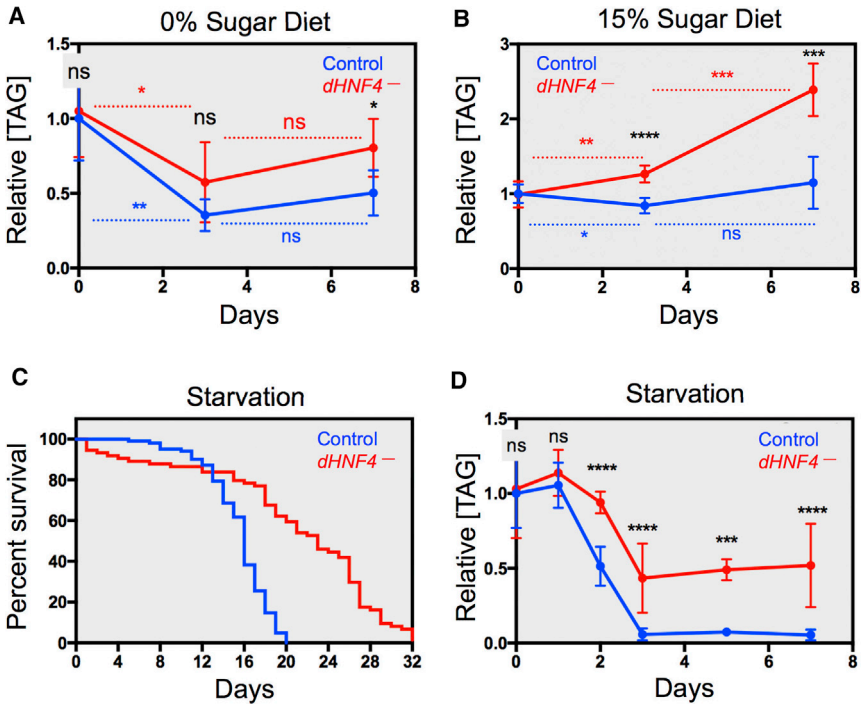

Figure 2. *dHNF4* Suppresses Hyperlipidemia in Young Adults

(A and B) Triglyceride (TAG) levels were measured in 0 day, 3 day, or 7-day-old controls (blue) and *dHNF4* mutants (red) reared on a 0% sugar diet and transferred to a 0% (A) or a 15% (B) sugar diet after adult emergence. TAG levels are normalized to total protein and represented relative to the level in 0-day controls. Black asterisks represent statistically significant differences between controls and mutants at a given time point, while red or blue asterisks represent statistically significant differences between two time points for either controls or mutants.

(C) Lifespan was scored for control and *dHNF4* mutants upon starvation under humid conditions. Animals were reared on a 0% sugar diet as larvae and starved at emergence. Median lifespans—controls: 16 days (n = 102); *dHNF4* mutants: 23 days (n = 74); $p < 0.0001$.

(D) Triglyceride (TAG) levels were measured in 0-, 1-, 2-, 3-, 5-, or 7-day old controls (blue) and *dHNF4* mutants (red) reared on a 0% sugar diet and starved at emergence under humid conditions. TAG levels are not normalized to protein because protein diminishes upon starvation (Figure S1B). Data are presented relative to the level in 0-day-old controls. The asterisks represent statistically significant differences between controls and *dHNF4* mutants at a given time point.

See also Figure S1.

newly emerged adults are eliminated normally in starved *dHNF4* mutants (Figures S2A and S2B). Similarly, the rate of TAG clearance in the hemolymph of both starved and fed young adults appears largely unaffected (Figure S2C). Staining with the lipophilic dye Oil Red O revealed that neutral lipids are progressively lost in larval adipose cells and the fat body of starved controls (Figure 3A, upper and middle panels). A similar pattern is seen in the fat bodies of *dHNF4* mutants; however, lipids accumulate rapidly in oenocytes, which are specialized lipid metabolizing cells embedded in the adult fat tissue (Figure 3A, lower panels) (Gutierrez et al., 2007; Makki et al., 2014). This steatosis persists for at least 14 days of starvation (Figure S2D). In contrast, the oenocytes in controls contain small lipid droplets at emergence, which are cleared within 2 days of starvation (red arrowhead, Figure 3A, middle panels). Lipid accumulation in the oenocytes of *dHNF4* mutants occurs independently of nutritional status, as it is also observed in animals fed a 0% or a 15% sugar diet (Figure 3B).

dHNF4 Functions in Oenocytes to Maintain Lipid Homeostasis

Antibody stains reveal that *dHNF4* is expressed at high levels in oenocytes, with low levels of expression in the neighboring adult adipose tissue (Figure S3A). Silencing of *dHNF4* expression in oenocytes using the *PromE-Gal4* driver and a *UAS-dHNF4 RNAi* transgene results in lipid accumulation in oenocytes in both starved and fed animals (Figures 4A and S3B). A similar result is seen in the oenocytes of starved females, indicating that steatosis is not a remote effect from *dHNF4* RNAi in male accessory glands, where the *PromE-Gal4* driver is also expressed (Figure S3C) (Billeter et al., 2009; Bousquet et al., 2012). Conversely, expression of wild-type *dHNF4* in the oenocytes of *dHNF4* mutants rescues lipid accumulation in these cells, as well as TAG clearance upon starvation (Figures 4B, 4C, and S3D). These results demonstrate that *dHNF4* acts in oenocytes to suppress lipid accumulation in these cells and to maintain systemic lipid homeostasis in starved animals.

Impaired Fatty Acid Elongation Contributes to Developmental Steatosis in *dHNF4* Mutant Oenocytes

Oenocyte-specific RNAi directed against key genes in the fatty acid β-oxidation pathway does not lead to steatosis, demonstrating that this phenotype does not arise from a defect in lipid catabolism (Figure S4A). Rather, *dHNF4* might be required for the proper production of VLCFAs and their derivatives called hydrocarbons, which are the primary products of adult oenocytes (Billeter et al., 2009; Makki et al., 2014; Parvy et al., 2012; Wicker-Thomas et al., 2015). Hydrocarbons are secreted to the overlying epidermis and cuticle where they act as pheromones and waterproofing agents (Makki et al., 2014; Wicker-Thomas et al., 2015; Wigglesworth, 1988). Briefly, VLCFA/hydrocarbon biosynthesis starts with palmitate, which is synthesized by ACC and FASN (Figure 5A). This fatty acid is elongated by the successive action of elongase, KAR, HACD, and TER enzymes, before being converted to hydrocarbons (Cinnamon et al., 2016; Qiu et al., 2012; Wicker-Thomas et al., 2015). Analysis of previous RNA sequencing (RNA-seq) data indicates that the transcription of genes involved in VLCFA and hydrocarbon biosynthesis, including *KAR*, *Cyp4g1*, *Cpr*, and many elongases, is reduced in mature adults lacking *dHNF4* function (Figure S4B) (Barry and Thummel, 2016). We validated these results in young starved adults by RT-qPCR (Figure 5B). The expression of

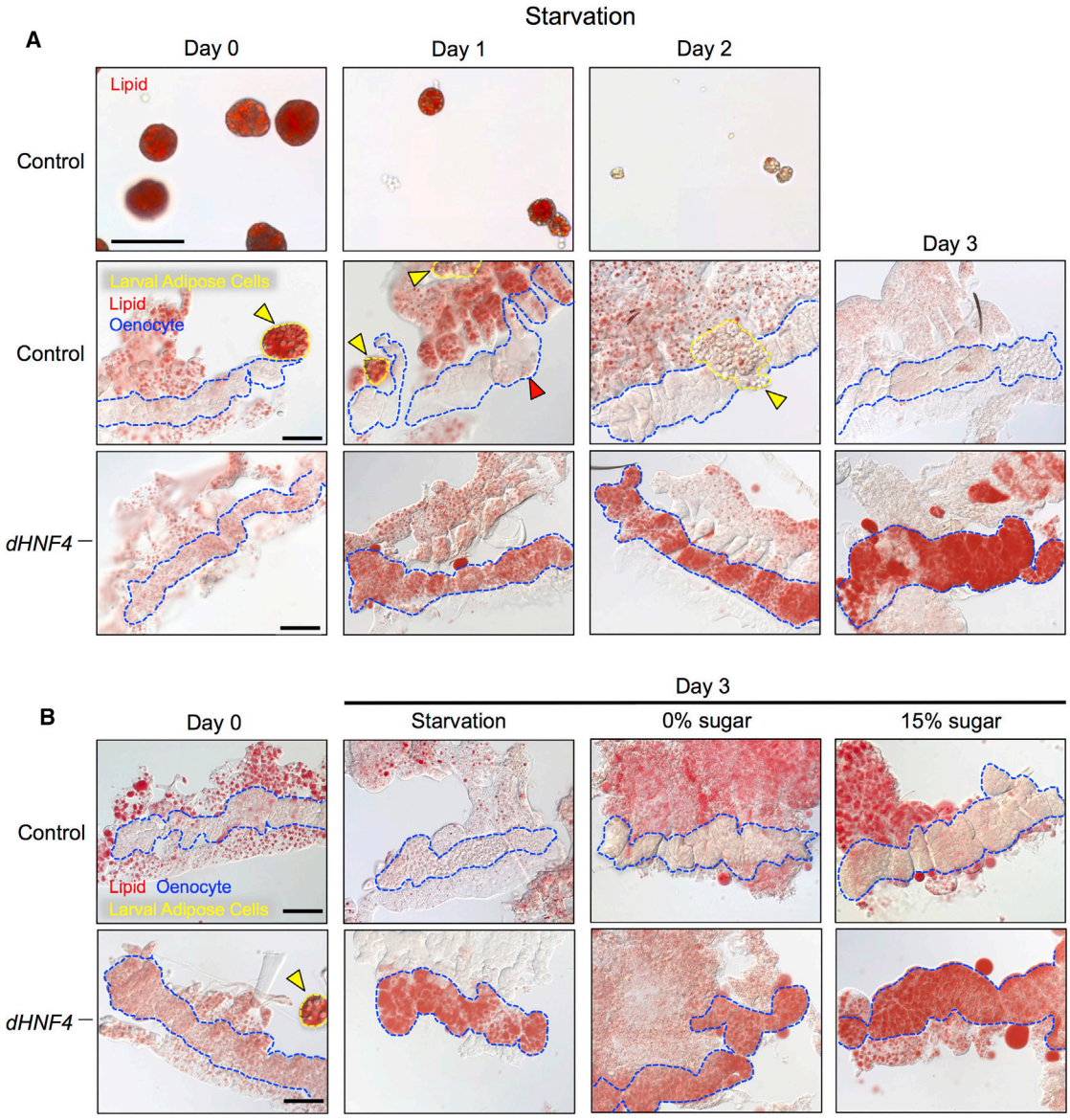

Figure 3. Oenocytes Become Steatotic at the Onset of Adulthood in *dHNF4* Mutants

(A) Oil Red O stains are depicted for larval adipose cells of starved control adults (upper panels), oenocytes and adult fat bodies of starved controls (middle panels), and *dHNF4* mutants (lower panels). Animals were reared on a 0% sugar diet as larvae and starved after emergence under humid conditions.

(B) Oil Red O stains are depicted for oenocytes and fat bodies of control and *dHNF4* mutants at emergence (day 0) or in 3-day-old animals that were either starved or fed a 0% or 15% sugar diet after emergence.

(A and B) Oenocytes are outlined with a blue dotted line. Larval adipose cells (individual cells or aggregates) are outlined with a yellow dotted line and indicated with a yellow arrowhead. The red arrowhead in day 1 controls indicates small persisting lipid droplets in control oenocytes at this time. Scale bars: 50 μm.

See also Figure S2.

dHNF4, *ACC*, *KAR*, *Cpr*, *Cyp4g1*, and three genes encoding elongases (*CG30008, CG18609, and CG16904*) is induced after emergence and peaks at day 2 in controls, indicating that VLCFA/hydrocarbon biosynthesis is activated shortly after this developmental transition. This induction is blunted in the absence of *dHNF4*, with major effects on *KAR*, *Cpr*, *CG30008*, and *CG18609*. *dHNF4* is thus required for the developmental induction of key genes in the VLCFA/hydrocarbon biosynthetic pathway at the onset of adulthood. Consistent with this, oenocyte-specific expression of *dHNF4* in *dHNF4* mutants is sufficient to rescue *KAR* and *CG18609* transcript levels (Figure S4C). The expression of *CG30008*, however, remains unaffected, suggesting that other tissues can also direct fatty acid elongation in a *dHNF4*-dependent manner.

The reduced expression of genes involved in VLCFA/hydrocarbon synthesis could contribute to oenocyte steatosis in *dHNF4* mutants. Consistent with this possibility, we observed lipid accumulation in the oenocytes of young adults that carry

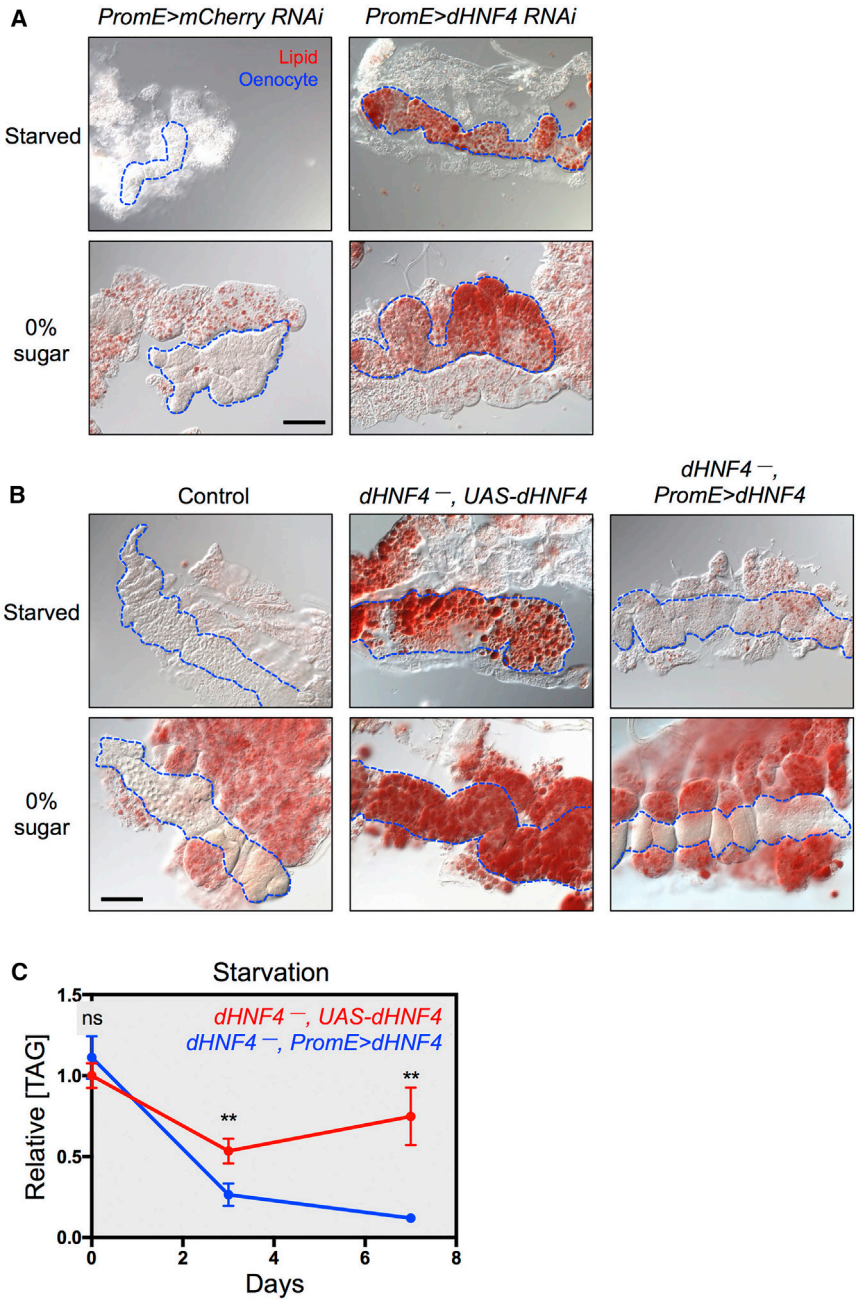

Figure 4. *dHNF4* Acts in Oenocytes to Suppress Steatosis

(A) Oil Red O stains are depicted for oenocytes and fat bodies of 7-day-old controls (*PromE>mCherry RNAi*) and 7-day-old animals with oenocyte-specific *dHNF4* RNAi (*PromE> dHNF4 RNAi*). Animals were raised on a 0% sugar diet and starved or fed a 0% sugar diet after emergence.

(B) Oil Red O stains are depicted for oenocytes and fat bodies of starved and fed 7–day-old controls, *dHNF4* mutants (*dHNF4*$^{-}$, *UAS-dHNF4*), and *dHNF4* mutants with oenocyte-specific *dHNF4* rescue (*dHNF4*$^{-}$, *PromE>dHNF4*). Animals were raised on a 0% sugar diet and starved or fed a 0% sugar diet after emergence.

(A and B) Oenocytes are outlined with a blue dotted line. Scale bar: 50 μm.

(C) Triglyceride (TAG) levels were measured in 0-day-, 3-day-, or 7-day-old *dHNF4* mutants (*dHNF4*$^{-}$, *UAS-dHNF4*, red) and in *dHNF4* mutants with oenocyte-specific *dHNF4* rescue (*dHNF4*$^{-}$, *PromE>dHNF4*, blue). Animals were reared on a 0% sugar diet and starved at adult emergence under humid conditions. TAG levels are normalized to total protein and represented relative to the amount in 0-day *dHNF4* mutants. Black asterisks represent statistically significant differences between *dHNF4* mutants and *dHNF4* mutants with oenocyte-specific rescue at a given time point. See also Figure S3.

the *PromE-Gal4* driver in combination with a UAS-KAR *RNAi* transgene (Figure 5C). *PromE-Gal4*-driven expression of *ACC*, *FASN*^{CG17374}, *Cpr,* and *Cyp4g1* RNAi transgenes was fully lethal between larval stages and adult emergence, as previously reported (Garrido et al., 2015; Gutierrez et al., 2007; Parvy et al., 2012). To circumvent this lethality, we used the *PromE-Gal4*, *Tub-Gal80*^{ts} driver, which allows temperature-inducible RNAi expression in oenocytes. As expected, no developmental lethality was observed when animals were left to develop at the permissive temperature (21°C). Shifting newly emerged adults to the restrictive temperature (29°C) led to mild oenocyte steatosis upon *ACC* RNAi, indicating that malonyl-CoA production and downstream fatty acid elongation is required to suppress lipid accumulation (Figure 5D). Adult-specific oenocyte RNAi for *FASN*^{CG17374}, *Cpr,* and *Cyp4g1*, however, did not lead to oenocyte steatosis, while RNAi for *KAR* led to reduced but detectable lipid accumulation relative to our results with the constitutively active *PromE-Gal4* driver (Figures 5C and 5D). Steatosis is also observed with a second *KAR* RNAi transgene (*KAR RNAi*$^{\#2}$), which was lethal prior to adulthood when driven with *PromE-Gal4*. In addition, adult-specific *dHNF4* RNAi led to abundant lipid accumulation in oenocytes, demonstrating that *dHNF4* is required after emergence to suppress steatosis at the onset of adulthood (Figure 5D). Similar results were seen with adults fed a 0% sugar diet (Figure S4D). Taken together, these results suggest that the reduced expression of genes involved in VLCFA elongation (*ACC* and *KAR*) is responsible for the steatosis observed in the oenocytes of *dHNF4* mutants following adult emergence.

dHNF4 Mutants Have Reduced Levels of Hydrocarbons and Are Sensitive to Dehydration

If the VLCFA/hydrocarbon biosynthetic pathway is impaired in newly emerged *dHNF4* mutants, then we should see reduced hydrocarbon production. To test this hypothesis, we used small-molecule gas chromatography-mass spectrometry (GC-MS) to

measure hydrocarbon levels in controls and *dHNF4* mutants at emergence, and in 3-day-old fed and starved animals (Figures 6A and S5A). Consistent with the temporal profile of VLCFA/hydrocarbon biosynthetic gene expression, most hydrocarbons are either low or absent at emergence but increase in 3-day-old controls. This can be seen for 7(Z)-tricosene, tricosane, and 7(Z)-pentacosene, which are abundant in males, along with 7(Z), 11(Z)-heptacosadiene, and a number of other hydrocarbons (Figures 6A and S5A) (Everaerts et al., 2010). Importantly, hydrocarbons are produced in starved controls, suggesting that pre-existing larval fat stores provide an important source of precursors for this pathway. Dietary input, however, is required for maximal hydrocarbon biosynthesis, as levels increase in fed adults (Figures 6A and S5A). Interestingly, the synthesis of some hydrocarbon species could rely specifically on dietary lipids, as suggested by the major increases in tricosene 3, heneicosane, and hydrocarbon 2 in 3-day-old fed controls relative to starved animals (Figure S5A). In addition, a few hydrocarbons are already present at moderate levels at emergence, suggesting that they are synthesized at an earlier developmental stage and carried over into the young adult (7(Z), 11(Z)-heptacosadiene, nonacosene, and hydrocarbon 2; Figures 6A and S5A). Importantly, many hydrocarbons are significantly reduced in fed or starved *dHNF4* mutants, demonstrating that this nuclear receptor is required for proper hydrocarbon biosynthesis. In contrast, heneicosane levels are unaffected by a loss of *dHNF4* function suggesting that this hydrocarbon is produced through a distinct pathway (Figure S5A).

The hydrophobic properties of hydrocarbons reduce trans-epidermal water loss and play a major role in desiccation resistance (Qiu et al., 2012; Wicker-Thomas et al., 2015). Consistent with this function, *dHNF4* mutants die significantly faster than controls when challenged by dry starvation in the absence of both food and water (Figures 6B and S5B). *dHNF4* silencing in oenocytes recapitulates this desiccation sensitivity, and oenocyte-specific expression of wild-type *dHNF4* in mutants rescues this phenotype (Figures 6C and 6D). Moreover, *dHNF4* mutants lose more water than controls when exposed to dry conditions, but fluid homeostasis is rapidly restored when these animals are returned to a humid environment (Figure 6E). We further tested for defects in the hydrophobic coating of the cuticle by collecting dead dry control and *dHNF4* mutant flies following dry starvation and incubating them in water. While control carcasses remain at the surface of the liquid following a 2.5-hr incubation, *dHNF4* mutant carcasses sink below the surface (Figure S5C). After a 24-hr incubation in water, *dHNF4* mutant carcasses swell because of passive incorporation of liquid, while only mild fluid incorporation is seen in control carcasses (Figure 6F). In addition, the expression of *dHNF4* in the oenocytes of *dHNF4* mutants blocks passive water incorporation in dried carcasses (Figure S5D). Taken together, these results demonstrate that *dHNF4* is required in oenocytes for cuticular hydrophobicity, reducing trans-epidermal water loss, and providing tolerance to dry conditions.

Interestingly, mouse mutants for *Elovl1* and *Elovl4*, which encode fatty acid elongases, die shortly after birth from acute dehydration and display a loss of epidermal hydrophobic barrier function (Cameron et al., 2007; Sassa et al., 2013). This observation raises the possibility that the regulatory link between VLCFA biosynthesis and HNF4 may be conserved through evolution. To test this hypothesis, we examined the expression levels of several fatty acid elongase genes in both control and *HNF4α* mutant mouse hepatocytes, where they are normally abundantly expressed (Moon et al., 2009, 2014; Wang et al., 2006). Specific loss of *HNF4α* in mature hepatocytes results in significant reductions in *KAR*, *Elovl3,* and *Elovl5* mRNA levels (Figure 6G). Interestingly, the transcriptional level of *Elovl6* is elevated in *HNF4α* mutant hepatocytes, suggesting that the receptor regulates specific steps in the VLCFA biosynthetic pathway. We conclude that the regulation of VLCFA biosynthesis is an evolutionarily conserved function for HNF4.

dHNF4 Acts in Oenocytes to Suppress Sugar Toxicity

The central role of *dHNF4* in oenocyte function and lipid metabolism at the onset of adulthood raises the possibility that these activities could contribute to the reduced lifespan of *dHNF4* mutants (Figure 1). As a first step toward testing this hypothesis, we examined the lifespan of either control adults (*PromE>mCherry RNAi*) or animals with oenocyte-specific *dHNF4* RNAi (*PromE>dHNF4 RNAi*) maintained on a sugar-free diet, or raised on this diet and then transferred to 15% sugar after emergence (Figure 7A). As seen in our earlier study of *dHNF4* mutants (Figure 1A), controls display an increased lifespan in response to dietary sugar (solid blue curve, Figure 7A). In contrast, *dHNF4* RNAi animals display a major reduction in lifespan, demonstrating that *dHNF4* is required in oenocytes to suppress sugar toxicity (solid red curve, Figure 7A). Of note, controls and *dHNF4* RNAi animals have similar survival curves on a sugar-free diet (dotted blue and red curves, median lifespans: 31 days and 36 days, respectively, $p = 0.502$; log-rank Mantel-Cox test) (Figure 7A). Moreover, oenocyte-specific expression of wild-type *dHNF4* in mutants dramatically prolongs the lifespan of adults transferred to a 15% sugar diet and partly rescues their metabolic defects (purple in Figures 7B and 7C). Consistent with the absence of lipid accumulation in oenocytes (Figure 4B), oenocyte-specific *dHNF4* rescue reduces triglyceride levels in mutants (Figure 7C). These levels, however, remain elevated relative to controls, suggesting that *dHNF4* acts in multiple tissues to maintain systemic lipid homeostasis. Similarly, oenocyte-specific *dHNF4* rescue partly rescues the elevated glucose levels seen in mutants (Figure 7C). *dHNF4* is thus required in oenocytes for maintaining triglyceride and glucose homeostasis, as well as suppressing the deleterious effects of a sugar diet.

dHNF4 is required in oenocytes for hydrocarbon production, suppressing dietary sugar toxicity and maintaining glucose homeostasis, raising the possibility that these physiological processes are linked. In support of this hypothesis, adult-specific silencing of several genes involved in hydrocarbon biosynthesis (*PromE-Gal4, tub-Gal80^{ts}*, *>ACC*, *>KAR*, or *>Cyp4g1* RNAi) leads to elevated glucose levels and reduces the longevity of animals raised on a 15% sugar diet (Figures 7D, 7E, S6A, and S6B). Importantly, these physiological defects appear to be linked to the inability to maintain fluid homeostasis. Raising animals with oenocyte-specific *Cyp4g1* RNAi induced at emergence in high humidity restores both their longevity and systemic glucose levels when fed a 15% sugar diet (Figures 7D and 7E). Similarly, humidity is sufficient to rescue the sensitivity of *dHNF4* mutants to a sugar diet. Increasing humidity on a sugar-free diet has little

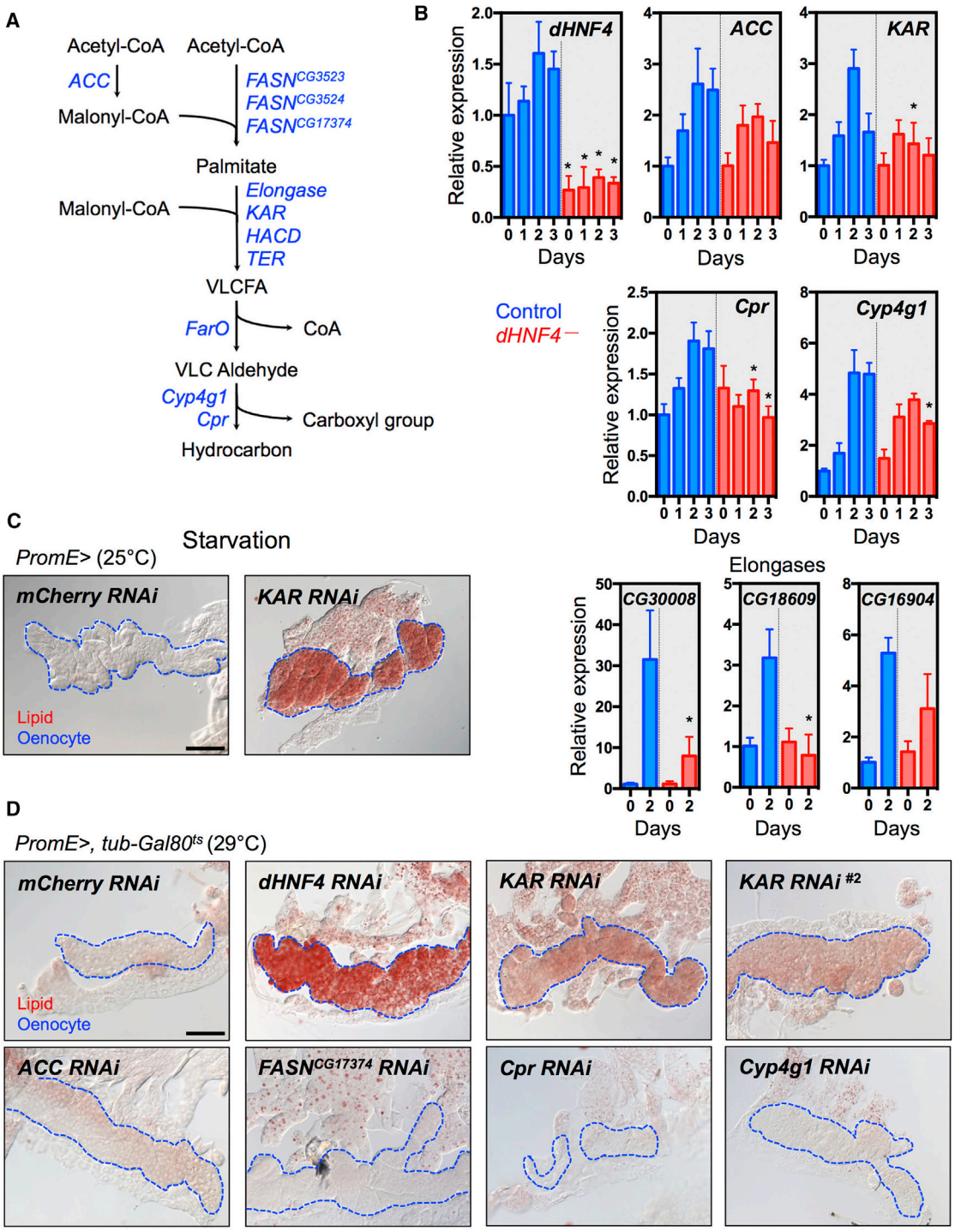

Figure 5. *dHNF4* Is Required for the Proper Expression of Genes Involved in VLCFA and Hydrocarbon Synthesis

(A) A simplified representation of the VLCFA and hydrocarbon biosynthetic pathway is depicted along with the *Drosophila* genes (in blue) that encode key enzymes in this pathway. Elongase, HACD, and TER are each encoded by multiple genes.

(B) RT-qPCR analysis of *dHNF4* mRNA and transcripts encoding key steps in the VLCFA/hydrocarbon metabolic pathway in starved controls (blue bars) and starved *dHNF4* mutants (red bars) after adult emergence. Transcript levels were analyzed at 0, 1, 2, and 3 days or 0 and 2 days after adult emergence. Transcript levels are normalized to *rp49* mRNA and presented relative to the level in day 0 controls. Asterisks represent statistically significant differences with control transcripts at the same time point.

(C) Oil Red O stains are depicted for oenocytes and adult fat bodies from 7-day-old starved controls (*PromE>mCherry RNAi*) and animals with oenocyte-specific *KAR* RNAi (*PromE> KAR RNAi*) reared at 25°C.

(legend continued on next page)

effect on the lifespan of *dHNF4* mutants (Figure 7F, pink curves), while the same conditions on a 15% sugar diet dramatically prolong mutant lifespan (Figure 7F, red curves), with animals surviving longer than those fed a sugar-free diet (Figure 7F, right panel). In addition, humidity prolongs the lifespan of animals with oenocyte-specific loss of *dHNF4* function on a 15% sugar diet, while it has no significant effect on the lifespan of mutants with oenocyte-specific *dHNF4* rescue (Figures S6C and S6D). This indicates that increased humidity specifically compensates for the defects associated with the loss of *dHNF4* in the oenocytes of animals with systemic *dHNF4* loss-of-function. Finally, we found that while increased humidity has no effect on glycogen or TAG levels in *dHNF4* mutants transferred to a 15% sugar diet at emergence, it restores their elevated glucose levels (Figures 7G and S6E). Taken together, our results support the model that the inability of *dHNF4* mutants to produce hydrocarbons and maintain systemic fluid homeostasis contributes to their dietary sugar sensitivity and defects in glucose homeostasis.

DISCUSSION

dHNF4 Is Required to Coordinate VLCFA/Hydrocarbon Production with Adult Emergence

Drosophila breeds and feeds on rotting fruits, which are ephemeral ecosystems. Thus, while the *Drosophila* larva lives inside a semi-liquid nutritive substrate and feeds extensively to support its rapid increase in mass, the mature adult fly emerges into an unpredictable environment where it uses flight for dispersal and the colonization of more favorable niches. Similar to all insects, the large surface-to-volume ratio of *Drosophila* adults makes them vulnerable to dehydration (Albers and Bradley, 2004). In addition, the metabolic demands of flight require a high rate of gas exchange via the respiratory system, increasing water loss (Lehmann, 2001). We show here that the successful transition from a stationary and protected pupa to a motile adult that can survive in a dry environment is dependent on the dHNF4 nuclear receptor, which acts in the oenocytes to direct a transcriptional program that supports the rapid production of VLCFAs and cuticular hydrocarbons. This activity is consistent with earlier studies, which have demonstrated an important role for oenocytes in VLCFA/hydrocarbon synthesis and desiccation resistance, and places dHNF4 as a central transcriptional regulator for oenocyte function (Chatterjee et al., 2014; Chiang et al., 2016; Cinnamon et al., 2016; Köhler et al., 2009; Makki et al., 2014; Qiu et al., 2012; Wicker-Thomas et al., 2015).

One of the few larval tissues to escape autophagic cell death during metamorphosis is the larval fat body, which dissociates into individual adipose cells in prepupae (Nelliot et al., 2006). These cells persist through metamorphosis as free-floating larval cells within the hemolymph of the animal and begin to clear at adult emergence, with complete loss by day 2 of adulthood due to apoptosis (Aguila et al., 2007; Butterworth, 1972; Figures S2A–S2C). The larval adipose cells have been proposed to act as an energy reserve for the newly emerged adult, prior to feeding (Aguila et al., 2007). In support of this, newly emerged adults are more starvation resistant than mature adults (Aguila et al., 2007). We show, however, that whole-body and hemolymph TAG levels drop to low levels between emergence and day 3 of adulthood, on either a sugar-free diet or a rich 15% sugar diet (Figures 2A, 2B, and S2C). The lipids contained in larval adipose cells thus appear to be consumed independently of nutritional input, suggesting that they contribute to non-energetic functions. Moreover, control adults can survive for weeks in the absence of stored lipids, further indicating that they provide a relatively minor source of energy at this stage in development (Figures 2C and 2D).

We propose that lipids in the newly emerged adult are shunted toward a purpose that is more profound than energy production at this stage in development—the formation of a waterproof cuticle—and that this occurs in a *dHNF4*-dependent manner. Stored lipid levels are unaffected in newly emerged *dHNF4* mutant adults relative to controls (Figures 2A and 2B). Lipids, however, accumulate rapidly after this stage in oenocytes, in the presence or absence of nutrients, representing a developmental role for *dHNF4* in maintaining lipid homeostasis in this cell type (Figures 3A and 3B). The timing of lipid accumulation in the oenocytes of starved and fed *dHNF4* mutants coincides with the timing of lipid loss and larval adipose cell death (Figures 3A, 3B, and S2A–S2C). Our genetic studies demonstrate that *dHNF4* is specifically required in oenocytes to suppress developmental steatosis (Figures 4A and 4B). This appears to be due to its role in inducing the expression of genes involved in VLCFA elongation. Oenocyte-specific silencing of *KAR* or *ACC* recapitulates the developmental steatotic phenotype, while silencing genes that encode downstream or upstream steps in the hydrocarbon biosynthetic pathway (*FASN*^{CG17374}, *Cpr*, or *Cyp4g1*) has no effect on the lipid levels in oenocytes (Figures 5C, 5D, and S4D). Further studies are needed to determine the molecular mechanisms that link VLCFA elongation with oenocyte lipid homeostasis. Finally, adults normally emerge with low hydrocarbon levels that increase dramatically over 3 days, even in the absence of food, in agreement with the hypothesis that the larval adipose cells provide the primary source of precursors for hydrocarbon production (Figures 6A and S5A). These results are consistent with previous reports, which have shown that dietary manipulation during larval life affects the blend of hydrocarbons in young adults (Stefana et al., 2017; Wicker-Thomas et al., 2015). Altogether, these observations support the model that *dHNF4* mediates the rapid conversion of persisting larval fat stores into hydrocarbons shortly after adult emergence.

Drosophila continuously shed and produce hydrocarbons throughout adulthood, indicating that this biosynthetic pathway is active at later stages to maintain a hydrophobic cuticle (Stefana et al., 2017). Consistent with this, we find that oenocyte-specific *dHNF4* RNAi in mature adults leads to a similar degree

(D) Oil Red O stains are shown for oenocytes and adult fat bodies from 3- to 5-day-old starved controls (*mCherry RNAi*) and starved animals with adult-specific RNAi for *dHNF4*, *KAR, ACC, FASN*^{CG17374}, *Cpr*, or *Cyp4g1* in oenocytes using *PromE>, Tub-Gal80*^{ts}. Animals were kept at room temperature during larval development and starved at 29°C after emergence.

(C and D) Oenocytes are outlined with a blue dotted line. Scale bars: 50 μm.

See also Figure S4.

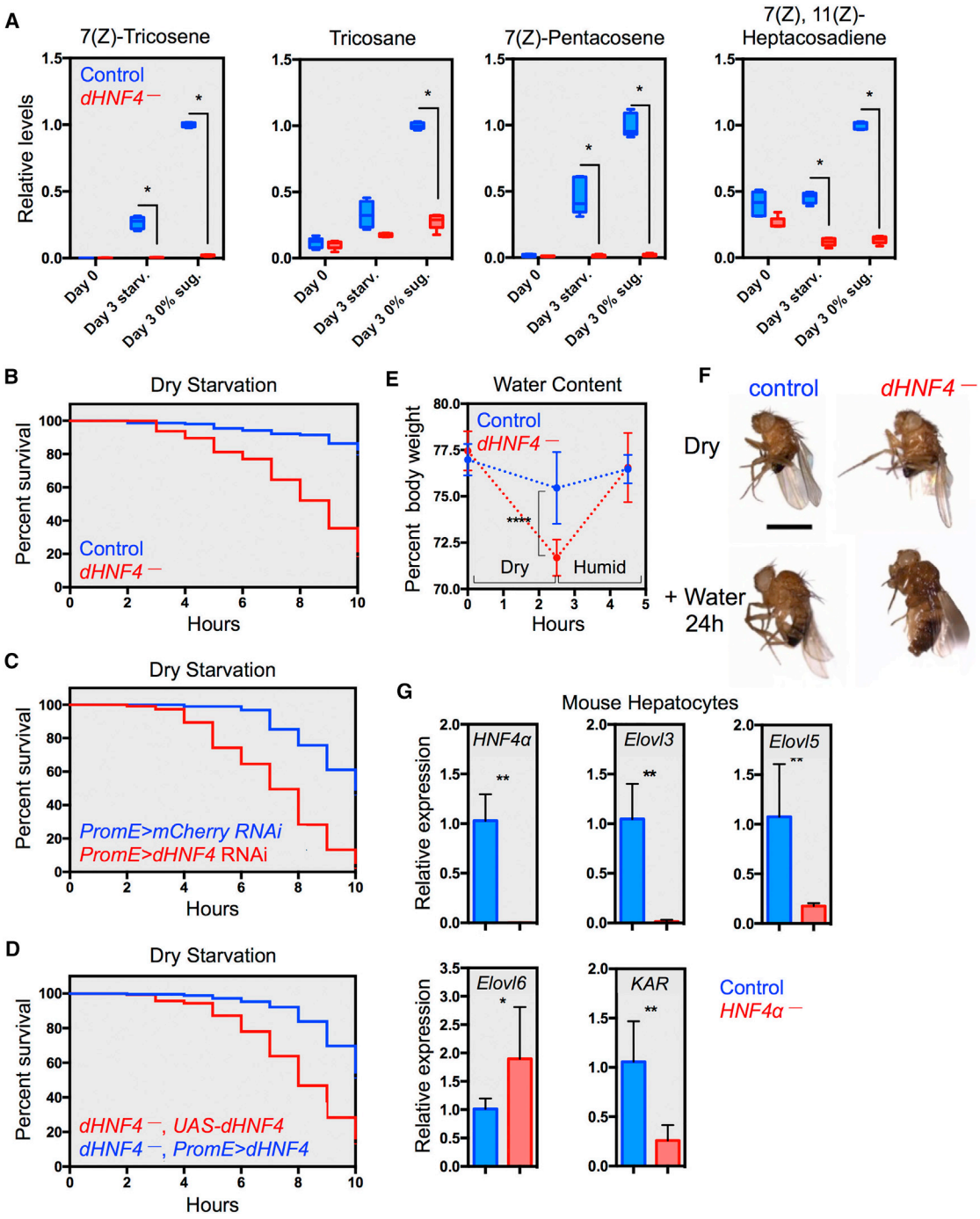

Figure 6. *dHNF4* Is Required for Hydrocarbon Production and Tolerance to Desiccation in Newly Emerged Adults

(A) Hydrocarbon levels are depicted as determined by GC-MS at emergence (day 0), in 3-day-old starved flies, and in 3-day-old flies fed a 0% sugar diet for both controls and *dHNF4* mutants. Values are presented relative to the amount in 3-day-old fed controls. The identity of each hydrocarbon was confirmed by comparison with purified standards.

(B) Longevity was scored for controls and *dHNF4* mutants starved in the absence of water. Median lifespans—controls: 13 hr (n = 132) (extrapolated using control data from Figure S5B); *dHNF4* mutants: 9 hr (n = 48); $p < 0.0001$.

(C) Longevity was scored for controls (*PromE>mCherry RNAi*, blue) and animals with oenocyte-specific *dHNF4* RNAi (*PromE>dHNF4 RNAi*, red) in the absence of water. Median lifespans—controls: 10 hr (n = 95); *PromE>dHNF4 RNAi* animals: 7 hr (n = 113); $p < 0.0001$.

(D) Longevity was scored for *dHNF4* mutants (*dHNF4⁻, UAS-dHNF4*, red) and *dHNF4* mutants with oenocyte-specific *dHNF4* rescue (*dHNF4⁻, PromE>dHNF4*, blue) in the absence of water. Median lifespans—*dHNF4* mutants: 8 hr (n = 141); *dHNF4⁻, PromE>dHNF4* animals: >10 hr (n = 254); $p < 0.0001$.

(legend continued on next page)

of lipid accumulation as that seen upon inducing RNAi at emergence (Figure S7E). Further studies are required to address this continuing role for *dHNF4* in mature adults. In addition, the mechanisms that partition stored lipids toward VLCFA/hydrocarbon production or energy production remain to be determined. Finally, the key functions we describe for *dHNF4* in oenocytes are shared between males and females, indicating that they are not sex specific (Figures S3C and S7A–S7D).

Humid Conditions Are Required to Assess the Starvation Resistance of Adult *Drosophila*

Our studies of starvation resistance indicate that newly emerged *Drosophila* adults can tolerate the absence of nutrients for at least a week. During the non-feeding period of metamorphosis, pupae consume about half of their glycogen and TAG stores and most of the trehalose gathered during the larval stages (Matsuda et al., 2015). In spite of this depletion of energy reserves, sufficient nutrients persist to allow the newly emerged adult to survive and disperse in their new environment. Under hydrated conditions, control lines emerge with the ability to survive from 1 to 3 weeks in the absence of nutrients (Figures 2C and S1A). This contrasts with published data, most of which report survival of *Drosophila* adults for up to 3 days (Aguila et al., 2007; Chatterjee et al., 2014). These assays use either moist filter paper or PBS in 1% agar as a medium for starvation (Tennessen et al., 2014). We suggest that these conditions provide insufficient humidity to accurately distinguish the effects of dehydration from the effects of nutrient depletion. Without moisture or food, *Drosophila* die in less than a day, with a median lifespan of 13 hr (Figures 6B and S5B). Thus, as is well known in mammals, sufficient hydration is critical for assessing the ability of animals to properly mobilize stored nutrients for survival during starvation.

dHNF4 Regulates the Expression of Genes in the VLCFA/Hydrocarbon Biosynthetic Pathway

Changes in metabolism must accompany each stage in development in order to allow normal progression through the life cycle. Although little is known about how development and metabolism are coupled, nuclear receptors appear to play a central role in this process (Li and Tennessen, 2017). Consistent with this, our previous study of *dHNF4* showed that it is highly up-regulated at the end of metamorphosis as the fly begins its adult life, coordinately inducing genes involved in glucose homeostasis and oxidative phosphorylation (Barry and Thummel, 2016). Functional studies showed that *dHNF4* acts at this stage in the insulin-producing cells to maintain glucose-stimulated insulin secretion and acts in the fat body to promote glucose clearance. Here, we expand upon these activities for *dHNF4* at the onset of adulthood to include an essential role in supporting VLCFA and hydrocarbon production in the oenocytes to allow adult survival and dispersion.

Key genes involved in VLCFA/hydrocarbon production are induced at the onset of adulthood in control adults and reduced in expression in *dHNF4* mutants, including *KAR*, *Cpr*, *Cyp4g1*, and several genes encoding predicted elongases (Figures 5A and 5B). In addition, dHNF4 transcriptional activity can be activated by LCFAs and VLCFAs, which appear to act as ligands for this nuclear receptor (Palanker et al., 2009). This is consistent with studies of mammalian HNF4α, which have identified LCFAs as ligands that can trigger the conformational changes required for coactivator recruitment (Duda et al., 2004; Wisely et al., 2002; Yuan et al., 2009). Thus, the free fatty acids generated by lipolysis from the larval adipose cells could act as ligands for dHNF4 in oenocytes, driving the transcription of genes in the VLCFA/hydrocarbon pathway. The resulting VLCFAs might further activate dHNF4, providing a feed-forward loop to enhance VLCFA/hydrocarbon production. These levels of regulation could ensure that free fatty acids are rapidly and efficiently converted into VLCFAs and hydrocarbons to provide an effective waterproof barrier for the young adult.

dHNF4 Links Systemic Fluid Homeostasis with Tolerance to Dietary Sugars

Simple carbohydrates are required for optimal *Drosophila* longevity, yet *dHNF4* and VLCFA/hydrocarbon biosynthesis are required in oenocytes to provide tolerance to these nutrients (Figures 7A, 7B, 7D, and S6A). In addition, increased humidity is sufficient to rescue sugar toxicity and hyperglycemia in *dHNF4* mutants, suggesting that defects in fluid homeostasis are contributing to these phenotypes (Figures 7F and 7G). Defects in fluid homeostasis could occur in *dHNF4* mutants because of impaired waterproofing of the cuticle or the trachea. Parvy and colleagues demonstrated that, besides providing precursors for hydrocarbon synthesis, VLCFA metabolism in oenocytes is required to remotely waterproof the respiratory system in larvae (Parvy et al., 2012). Notably, disrupting VLCFA production in oenocytes via *ACC*, *KAR*, or *FASN*^{CG17374} RNAi in this cell type results in defects in tracheal waterproofing and larval lethality. We also observed lethality between larval and pupal stages when we drove these RNAi constructs with a constitutive oenocyte-specific GAL4 driver. However, we do not see defects in tracheal air filling or lethality in *dHNF4* mutant larvae or in animals with constitutive *dHNF4* RNAi expression in oenocytes, suggesting that there are no significant effects on tracheal waterproofing in these animals. In addition, altering cuticular hydrocarbon production while leaving VLCFA synthesis intact (by silencing *Cyp4g1* in oenocytes) induces sugar toxicity and defects in glucose homeostasis (Figures 7D and 7E). We thus postulate that reduced hydrocarbon production by oenocytes and altered

(E) The water content was determined in controls and *dHNF4* mutants after 2.5 hr of dry starvation (dry) followed by a 2-hr recovery in humid conditions (humid). No significant difference was observed between controls and *dHNF4* mutants before dry starvation and after recovery in humid conditions (respectively $p = 0.131$ and $p = 0.594$). More details can be found in the STAR Methods.

(F) Dead control and *dHNF4* mutants were collected following dry starvation and incubated in water with agitation. *dHNF4* mutants, but not controls, passively incorporate water and regain their initial shape after 24 hr of hydration. Scale bar: 1 mm.

(G) RT-qPCR analysis of *HNF4*α mRNA and transcripts corresponding to genes involved in VLCFA metabolism in control and *HNF4*α mutant mouse hepatocytes. Transcripts levels are normalized to *Rpl13* mRNA and presented relative to the levels in controls.

See also Figure S5.

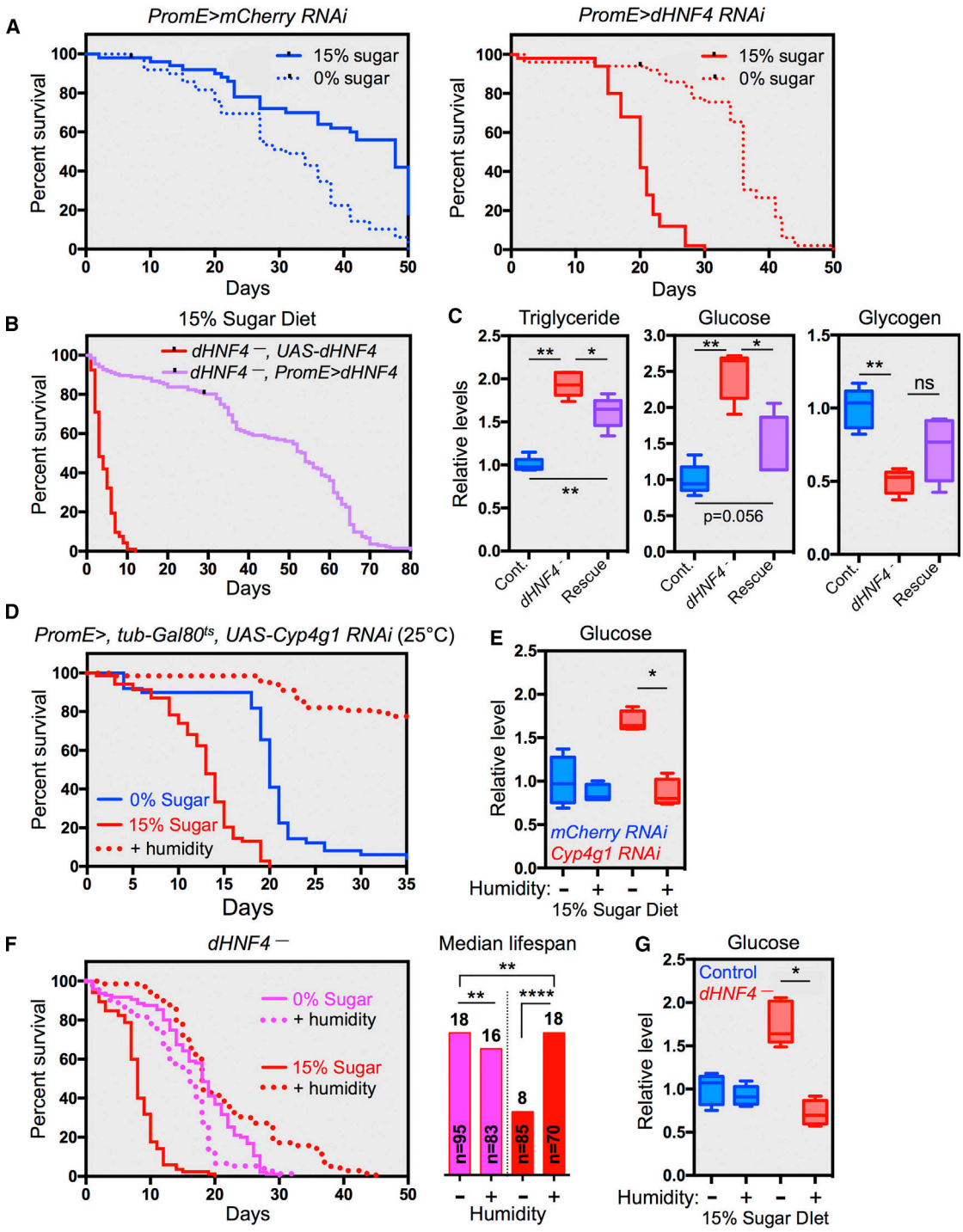

Figure 7. *dHNF4* Is Required in Oenocytes for Suppressing Dietary Sugar Toxicity and Maintaining Systemic Glucose Homeostasis

(A) Lifespan was scored for controls (*PromE>mCherry RNAi*, blue) and animals with oenocyte-specific *dHNF4* RNAi (*PromE>dHNF4 RNAi*, red) reared on a 0% sugar diet as larvae and transferred to a 0% or a 15% sugar diet after adult emergence (dotted and solid lines, respectively). Control median lifespan—0% sugar diet: 31 days (n = 49); 15% sugar diet: 48 days (n = 41); $p < 0.0001$. *PromE>dHNF4 RNAi* median lifespan—0% sugar diet: 36 days (n = 49); 15% sugar diet: 20 days (n = 50); $p < 0.0001$.

(B) Lifespan was scored for *dHNF4* mutants (*dHNF4*$^{-}$, *UAS-dHNF4*, red line) and *dHNF4* mutants with oenocyte-specific *dHNF4* rescue (*dHNF4*$^{-}$, *PromE>dHNF4*, purple line) reared on a 0% sugar diet as larvae and transferred to a 15% sugar diet after emergence. Median lifespan—*dHNF4* mutants: 3 days (n = 93), *dHNF4*$^{-}$, *PromE>dHNF4* animals: 54 days (n = 134); $p < 0.0001$.

(legend continued on next page)

cuticular waterproofing play central roles in the physiological defects we observe in *dHNF4* mutants.

Our understanding of diabetes in humans provides possible models to explain the physiological mechanisms that link *dHNF4* activity in oenocytes to fluid and carbohydrate homeostasis. In mammals, excess blood glucose cannot be effectively reabsorbed by the kidney and is excreted with urine (Lawrence, 1940). This induces osmotic diuresis (an increase in urination volume) to dilute the glucose osmolyte. Increased urination can lead to dehydration that further increases hyperglycemia and produces a hyperosmolar hyperglycemic state, which is a major contributor to diabetic mortality (Pasquel and Umpierrez, 2014; Rosenbloom, 2010). One possibility is that *dHNF4* mutants provide a sensitized genetic context for the development of a hyperosmolar hyperglycemic state in *Drosophila*. Increased transepidermal water loss could reduce hemolymph volume, contributing to the development of hyperglycemia on a sugar-containing diet. This hypothesis could explain the elevated glucose levels observed in *dHNF4* mutants and the normalization of glucose levels in high humidity. Further studies are required to test this possibility and dissect the mechanisms that couple *dHNF4* function in oenocytes to systemic carbohydrate homeostasis.

A number of studies have focused on characterizing the signaling pathways that govern glucose sensing and metabolism in *Drosophila* (Ghosh and O'Connor, 2014; Havula et al., 2013; Matsuda et al., 2015; Owusu-Ansah and Perrimon, 2014; Teleman et al., 2012). These studies have provided evidence for glucose-induced cellular damage via oxidative stress or the formation of advanced glycation end-products (Garrido et al., 2015; Teesalu et al., 2017). In spite of these efforts, however, more remains to be learned about the mechanisms underlying dietary sugar toxicity. Our work suggests unexpected roles for oenocyte lipid metabolism and hydration status in regulating glucose homeostasis and suppressing sugar toxicity in *Drosophila*.

Roles for HNF4 in the Synthesis of VLCFAs Are Conserved through Evolution

Interestingly, the role of VLCFAs in reducing trans-epidermal water loss is conserved through evolution (Nakamura et al., 2014). Mutations in genes encoding VLCFA acyl-CoA synthetases ACS-20 and ACS-22 result in disrupted cuticular barrier function and hypo-osmolality in *C. elegans* (Kage-Nakadai et al., 2010). Similarly, mouse mutants for *Elovl1* and *Elovl4* are born normally but die shortly thereafter from acute dehydration, similar to *dHNF4* mutant adults (Cameron et al., 2007; Li et al., 2007; McMahon et al., 2007; Sassa et al., 2013; Vasireddy et al., 2007). This lethality is accompanied by reduced epithelial barrier function, defects in the lamellar structure of newborn skin, reduced levels of VLCFAs, and the absence of key acylceramides that contribute to skin hydrophobicity. Genetic studies of the gene encoding ELOVL3, which elongates C20 fatty acids to C22 and C24, revealed similar functions. *Elovl3* mutant mice have disrupted skin and hair morphology resulting in increased trans-epidermal water loss (Westerberg et al., 2004). In addition, *Elovl5* and *Elovl6* mouse mutants display hepatic steatosis, similar to the lipid accumulation we see in *dHNF4* mutant oenocytes (Moon et al., 2009; Moon et al., 2014). Taken together, these results indicate that VLCFA production is critical for proper lipid metabolism and survival after birth in mouse, revealing a perinatal transition that parallels the role for VLCFAs and hydrocarbons in newly emerged *Drosophila* adults. Interestingly, our studies also link *Elovl* gene expression to *HNF4α* function in mice. We show that *Elovl3*, *Elovl5,* and *KAR* are all expressed at reduced levels in *HNF4α* mutant hepatocytes, indicating that this regulatory link is conserved through evolution (Figure 6G). Further studies are required to determine if *HNF4α* exerts a similar role in mammalian skin and if its activity is required for epithelial barrier function and desiccation resistance.

STAR★METHODS

Detailed methods are provided in the online version of this paper and include the following:

- KEY RESOURCES TABLE
- CONTACT FOR REAGENT AND RESOURCE SHARING
- EXPERIMENTAL MODEL AND SUBJECT DETAILS
  - *Drosophila* Strains and Handling
  - Fly Diets
  - *HNF4α* Mutant Mouse Hepatocytes
- METHOD DETAILS
  - Lifespan Studies on 0% and 15% Sugar Diets
  - Studies on Diets with Increased Humidity
  - Starvation
  - Dry Starvation

(C) Triglyceride, glucose, and glycogen levels were measured in 7-day-old controls (Cont.), *dHNF4⁻, UAS-dHNF4* mutants (*dHNF4⁻*) and *dHNF4* mutants with oenocyte-specific *dHNF4* rescue (Rescue) transferred to a 15% sugar diet after emergence. Metabolite levels are normalized to total protein and presented relative to the amount in control animals.

(D) Lifespan was scored for animals with oenocyte-specific *Cyp4g1* RNAi induced at emergence in different dietary and humidity conditions. Animals were reared as larvae on a 0% sugar diet at room temperature and transferred to a 0% sugar diet (blue line) or a 15% sugar diet (red lines) with or without increased humidity (red dotted and solid lines, respectively) at 25°C to induce RNAi expression. Median lifespan: 0% sugar diet: 20 days (n = 50), 15% sugar diet: 13 days (n = 70), 15% sugar diet with increased humidity: >35 days (n = 67), $p < 0.0001$.

(E) Glucose levels were measured in 7-day-old *PromE-GAL4, tub-Gal80^{ts}, UAS-mCherry* RNAi controls (*mCherry RNAi*, blue box), and animals with oenocyte-specific *Cyp4g1* RNAi induced at emergence (*Cyp4g1 RNAi*, red boxes) transferred to a 15% sugar diet with or without increased humidity after adult eclosion.

(F) Lifespan was scored for *dHNF4* mutants reared on a 0% sugar diet as larvae and transfered to a 0% sugar diet (pink) or a 15% sugar diet (red) with or without increased humidity (dotted and solid lines, respectively) after adult emergence. The panel on the right depicts the median lifespans (numbers above each bar) and number of animals examined.

(G) Glucose levels were measured in 7-day-old controls and *dHNF4* mutants reared on a 0% sugar diet and transferred to a 15% sugar diet at adult emergence, with or without increased humidity.

(E and G) Metabolite levels are normalized to total protein and presented relative to the amount in controls without increased humidity.

See also Figures S6 and S7.

- Fly Water Content Determination
- Metabolite Assays
- Larval Adipose Cell Counts
- GC/MS Hydrocarbon Analysis
- Oil Red O Stains
- Immunostaining to Detect dHNF4 Protein
- RT-qPCR
- cDNA Synthesis from *Drosophila* Tissues
- cDNA Synthesis from Mouse Hepatocytes
- Information Related to Experimental Design

- QUANTIFICATION AND STATISTICAL ANALYSIS
  - Graphical Representation and Statistical Analysis of the Data

SUPPLEMENTAL INFORMATION

Supplemental Information includes seven figures and one table and can be found with this article online at https://doi.org/10.1016/j.devcel.2018.11.030.

ACKNOWLEDGMENTS

The authors would like to thank the Bloomington Stock Center, the Transgenic RNAi Project (TRiP), FlyBase, B. Dauwalter, A. Gould, and B. Mollereau for providing fly stocks; M. Peltier for help with the lifespan assays; and F. Leulier for comments on the manuscript. Metabolomics analysis was performed at the Metabolomics Core Facility at the University of Utah, which is supported by the NIH (S10 OD016232-01, S10 OD021505-01, and U54 DK110858-01). G.S. was funded by fellowships from the Fondation pour la Recherche Medicale (FRM SPE 40181) and the Bettencourt Schueller Foundation, and this research was supported by the NIH (R01DK108941, C.S.T.).

AUTHOR CONTRIBUTIONS

C.S.T. supervised the work. G.S. designed and interpreted experiments with input from H.-J.N. G.S. and H.-J.N. performed the experiments. J.S. and C.J.V. generated the *HNF4α* mutant hepatocytes and produced cDNA. G.S. and C.S.T. wrote the paper.

DECLARATION OF INTERESTS

The authors declare no competing interests.

Received: July 9, 2018
Revised: October 9, 2018
Accepted: November 14, 2018
Published: December 13, 2018

REFERENCES

Aguila, J.R., Suszko, J., Gibbs, A.G., and Hoshizaki, D.K. (2007). The role of larval fat cells in adult Drosophila melanogaster. J. Exp. Biol. *210*, 956–963.

Albers, M.A., and Bradley, T.J. (2004). Osmotic regulation in adult Drosophila melanogaster during dehydration and rehydration. J. Exp. Biol. *207*, 2313–2321.

Aldahmesh, M.A., Mohamed, J.Y., Alkuraya, H.S., Verma, I.C., Puri, R.D., Alaiya, A.A., Rizzo, W.B., and Alkuraya, F.S. (2011). Recessive mutations in ELOVL4 cause ichthyosis, intellectual disability, and spastic quadriplegia. Am. J. Hum. Genet. *89*, 745–750.

Barry, W.E., and Thummel, C.S. (2016). The Drosophila HNF4 nuclear receptor promotes glucose-stimulated insulin secretion and mitochondrial function in adults. Elife *5*, e11183.

Billeter, J.C., Atallah, J., Krupp, J.J., Millar, J.G., and Levine, J.D. (2009). Specialized cells tag sexual and species identity in Drosophila melanogaster. Nature *461*, 987–991.

Bousquet, F., Nojima, T., Houot, B., Chauvel, I., Chaudy, S., Dupas, S., Yamamoto, D., and Ferveur, J.F. (2012). Expression of a desaturase gene, desat1, in neural and nonneural tissues separately affects perception and emission of sex pheromones in Drosophila. Proc. Natl. Acad. Sci. USA *109*, 249–254.

Burt Solorzano, C.M., and McCartney, C.R. (2010). Obesity and the pubertal transition in girls and boys. Reproduction *140*, 399–410.

Butterworth, F.M. (1972). Adipose tissue of Drosophila melanogaster, V. Genetic and experimental studies of an extrinsic influence on the rate of cell death in the larval fat body. Dev. Biol. *28*, 311–325.

Cahill, G.F.J. (2006). Fuel metabolism in starvation. Annu. Rev. Nutr. *26*, 1–22.

Cameron, D.J., Tong, Z., Yang, Z., Kaminoh, J., Kamiyah, S., Chen, H., Zeng, J., Chen, Y., Luo, L., and Zhang, K. (2007). Essential role of Elovl4 in very long chain fatty acid synthesis, skin permeability barrier function, and neonatal survival. Int. J. Biol. Sci. *3*, 111–119.

Catalano, P.M. (2010). Obesity, insulin resistance, and pregnancy outcome. Reproduction *140*, 365–371.

Chatterjee, D., Katewa, S.D., Qi, Y., Jackson, S.A., Kapahi, P., and Jasper, H. (2014). Control of metabolic adaptation to fasting by dILP6-induced insulin signaling in Drosophila oenocytes. Proc. Natl. Acad. Sci. USA *111*, 17959–17964.

Chen, W.S., Manova, K., Weinstein, D.C., Duncan, S.A., Plump, A.S., Prezioso, V.R., Bachvarova, R.F., and Darnell, J.E., Jr. (1994). Disruption of the HNF-4 gene, expressed in visceral endoderm, leads to cell death in embryonic ectoderm and impaired gastrulation of mouse embryos. Genes Dev. *8*, 2466–2477.

Chiang, Y.N., Tan, K.J., Chung, H., Lavrynenko, O., Shevchenko, A., and Yew, J.Y. (2016). Steroid hormone signaling is essential for pheromone production and oenocyte survival. PLoS Genet. *12*, e1006126.

Cinnamon, E., Makki, R., Sawala, A., Wickenberg, L.P., Blomquist, G.J., Tittiger, C., Paroush, Z., and Gould, A.P. (2016). Drosophila Spidey/Kar regulates oenocyte growth via PI3-kinase signaling. PLoS Genet. *12*, e1006154.

Duda, K., Chi, Y.I., and Shoelson, S.E. (2004). Structural basis for HNF-4α activation by ligand and coactivator binding. J. Biol. Chem. *279*, 23311–23316.

Everaerts, C., Farine, J.P., Cobb, M., and Ferveur, J.F. (2010). Drosophila cuticular hydrocarbons revisited: mating status alters cuticular profiles. PLoS One *5*, e9607.

Garrido, D., Rubin, T., Poidevin, M., Maroni, B., Le Rouzic, A.L., Parvy, J.P., and Montagne, J. (2015). Fatty acid synthase cooperates with glyoxalase 1 to protect against sugar toxicity. PLoS Genet. *11*, e1004995.

Ghosh, A.C., and O'Connor, M.B. (2014). Systemic activin signaling independently regulates sugar homeostasis, cellular metabolism, and pH balance in Drosophila melanogaster. Proc. Natl. Acad. Sci. USA *111*, 5729–5734.

Gutierrez, E., Wiggins, D., Fielding, B., and Gould, A.P. (2007). Specialized hepatocyte-like cells regulate Drosophila lipid metabolism. Nature *445*, 275–280.

Havula, E., Teesalu, M., Hyötyläinen, T., Seppälä, H., Hasygar, K., Auvinen, P., Orešič, M., Sandmann, T., and Hietakangas, V. (2013). Mondo/ChREBP-Mlx-regulated transcriptional network is essential for dietary sugar tolerance in Drosophila. PLoS Genet. *9*, e1003438.

Hayashi, Y., Mori, Y., Janssen, O.E., Sunthornthepvarakul, T., Weiss, R.E., Takeda, K., Weinberg, M., Seo, H., Bell, G.I., and Refetoff, S. (1993). Human thyroxine-binding globulin gene: complete sequence and transcriptional regulation. Mol. Endocrinol. *7*, 1049–1060.

Hayhurst, G.P., Lee, Y.H., Lambert, G., Ward, J.M., and Gonzalez, F.J. (2001). Hepatocyte nuclear factor 4alpha (nuclear receptor 2A1) is essential for maintenance of hepatic gene expression and lipid homeostasis. Mol. Cell. Biol. *21*, 1393–1403.

Kage-Nakadai, E., Kobuna, H., Kimura, M., Gengyo-Ando, K., Inoue, T., Arai, H., and Mitani, S. (2010). Two very long chain fatty acid acyl-CoA synthetase genes, acs-20 and acs-22, have roles in the cuticle surface barrier in Caenorhabditis elegans. PLoS One *5*, e8857.

Kelsey, M.M., and Zeitler, P.S. (2016). Insulin resistance of puberty. Curr. Diab. Rep. *16*, 64.

Köhler, K., Brunner, E., Guan, X.L., Boucke, K., Greber, U.F., Mohanty, S., Barth, J.M.I., Wenk, M.R., and Hafen, E. (2009). A combined proteomic and

genetic analysis identifies a role for the lipid desaturase Desat1 in starvation-induced autophagy in Drosophila. Autophagy *5*, 980–990.

Lawrence, R.D. (1940). Renal threshold for glucose: normal and in diabetics. Br. Med. J. *1*, 766–768.

Lehman, J.J., and Kelly, D.P. (2002). Transcriptional activation of energy metabolic switches in the developing and hypertrophied heart. Clin. Exp. Pharmacol. Physiol. *29*, 339–345.

Lehmann, F.O. (2001). Matching spiracle opening to metabolic need during flight in Drosophila. Science *294*, 1926–1929.

Li, H., and Tennessen, J.M. (2017). Methods for studying the metabolic basis of Drosophila development. Wiley Interdiscip. Rev. Dev. Biol. *6*, e280.

Li, J., Ning, G., and Duncan, S.A. (2000). Mammalian hepatocyte differentiation requires the transcription factor HNF-4alpha. Genes Dev. *14*, 464–474.

Li, W., Sandhoff, R., Kono, M., Zerfas, P., Hoffmann, V., Ding, B.C.-H., Proia, R.L., and Deng, C.X. (2007). Depletion of ceramides with very long chain fatty acids causes defective skin permeability barrier function, and neonatal lethality in ELOVL4 deficient mice. Int. J. Biol. Sci. *3*, 120–128.

Makki, R., Cinnamon, E., and Gould, A.P. (2014). The development and functions of oenocytes. Annu. Rev. Entomol. *59*, 405–425.

Matsuda, H., Yamada, T., Yoshida, M., and Nishimura, T. (2015). Flies without trehalose. J. Biol. Chem. *290*, 1244–1255.

McMahon, A., Butovich, I.A., Mata, N.L., Klein, M., Ritter, R., Richardson, J., Birch, D.G., Edwards, A.O., and Kedzierski, W. (2007). Retinal pathology and skin barrier defect in mice carrying a Stargardt disease-3 mutation in elongase of very long chain fatty acids-4. Mol. Vis. *13*, 258–272.

Miyazawa, H., and Aulehla, A. (2018). Revisiting the role of metabolism during development. Development *145*.

Moon, Y.A., Hammer, R.E., and Horton, J.D. (2009). Deletion of ELOVL5 leads to fatty liver through activation of SREBP-1c in mice. J. Lipid Res. *50*, 412–423.

Moon, Y.A., Ochoa, C.R., Mitsche, M.A., Hammer, R.E., and Horton, J.D. (2014). Deletion of ELOVL6 blocks the synthesis of oleic acid but does not prevent the development of fatty liver or insulin resistance. J. Lipid Res. *55*, 2597–2605.

Musselman, L.P., and Kühnlein, R.P. (2018). Drosophila as a model to study obesity and metabolic disease. J. Exp. Biol. *221* (Pt Suppl 1).

Nakamura, M.T., Yudell, B.E., and Loor, J.J. (2014). Regulation of energy metabolism by long-chain fatty acids. Prog. Lipid Res. *53*, 124–144.

Nelliot, A., Bond, N., and Hoshizaki, D.K. (2006). Fat-body remodeling in Drosophila melanogaster. Genesis *44*, 396–400.

Owusu-Ansah, E., and Perrimon, N. (2014). Modeling metabolic homeostasis and nutrient sensing in Drosophila: implications for aging and metabolic diseases. Dis. Model. Mech. *7*, 343–350.

Palanker, L., Tennessen, J.M., Lam, G., and Thummel, C.S. (2009). Drosophila HNF4 regulates lipid mobilization and beta-oxidation. Cell Metab. *9*, 228–239.

Parvy, J.P., Napal, L., Rubin, T., Poidevin, M., Perrin, L., Wicker-Thomas, C., and Montagne, J. (2012). Drosophila melanogaster acetyl-CoA-carboxylase sustains a fatty acid-dependent remote signal to waterproof the respiratory system. PLoS Genet. *8*, e1002925.

Pasquel, F.J., and Umpierrez, G.E. (2014). Hyperosmolar hyperglycemic state: A historic review of the clinical presentation, diagnosis, and treatment. Diabetes Care *37*, 3124–3131.

Qiu, Y., Tittiger, C., Wicker-Thomas, C., Le Goff, G.L., Young, S., Wajnberg, E., Fricaux, T., Taquet, N., Blomquist, G.J., and Feyereisen, R. (2012). An insect-specific P450 oxidative decarbonylase for cuticular hydrocarbon biosynthesis. Proc. Natl. Acad. Sci. USA *109*, 14858–14863.

Rosenbloom, A.L. (2010). Hyperglycemic hyperosmolar state: an emerging pediatric problem. J. Pediatr. *156*, 180–184.

Sassa, T., Ohno, Y., Suzuki, S., Nomura, T., Nishioka, C., Kashiwagi, T., Hirayama, T., Akiyama, M., Taguchi, R., Shimizu, H., et al. (2013). Impaired epidermal permeability barrier in mice lacking Elovl1, the gene responsible for very-long-chain fatty acid production. Mol. Cell. Biol. *33*, 2787–2796.

Simcox, J., Geoghegan, G., Maschek, J.A., Bensard, C.L., Pasquali, M., Miao, R., Lee, S., Jiang, L., Huck, I., Kershaw, E.E., et al. (2017). Global analysis of plasma lipids identifies liver-derived acylcarnitines as a fuel source for brown fat thermogenesis. Cell Metab. *26*, 509–522.e6.

Stefana, M.I., Driscoll, P.C., Obata, F., Pengelly, A.R., Newell, C.L., MacRae, J.I., and Gould, A.P. (2017). Developmental diet regulates Drosophila lifespan via lipid autotoxins. Nat. Commun. *8*, 1384.

Teesalu, M., Rovenko, B.M., and Hietakangas, V. (2017). Salt-inducible kinase 3 provides sugar tolerance by regulating NADPH/$NADP^+$ redox balance. Curr. Biol. *27*, 458–464.

Teleman, A.A., Ratzenböck, I., and Oldham, S. (2012). Drosophila: a model for understanding obesity and diabetic complications. Exp. Clin. Endocrinol. Diabetes *120*, 184–185.

Tennessen, J.M., Baker, K.D., Lam, G., Evans, J., and Thummel, C.S. (2011). The Drosophila estrogen-related receptor directs a metabolic switch that supports developmental growth. Cell Metab. *13*, 139–148.

Tennessen, J.M., Barry, W.E., Cox, J., and Thummel, C.S. (2014). Methods for studying metabolism in Drosophila. Methods *68*, 105–115.

Van Gilst, M.R., Hadjivassiliou, H., Jolly, A., and Yamamoto, K.R. (2005). Nuclear hormone receptor NHR-49 controls fat consumption and fatty acid composition in C. elegans. PLoS Biol. *3*, e53.

Vasireddy, V., Uchida, Y., Salem, N., Kim, S.Y., Mandal, M.N.A., Reddy, G.B., Bodepudi, R., Alderson, N.L., Brown, J.C., Hama, H., et al. (2007). Loss of functional ELOVL4 depletes very long-chain fatty acids (> or =C28) and the unique ω-O-acylceramides in skin leading to neonatal death. Hum. Mol. Genet. *16*, 471–482.

Wang, Y., Botolin, D., Xu, J., Christian, B., Mitchell, E., Jayaprakasam, B., Nair, M.G., Peters, J.M., Busik, J.V., Olson, L.K., et al. (2006). Regulation of hepatic fatty acid elongase and desaturase expression in diabetes and obesity. J. Lipid Res. *47*, 2028–2041.

Westerberg, R., Tvrdik, P., Undén, A.B., Månsson, J.E., Norlén, L., Jakobsson, A., Holleran, W.H., Elias, P.M., Asadi, A., Flodby, P., et al. (2004). Role for ELOVL3 and fatty acid chain length in development of hair and skin function. J. Biol. Chem. *279*, 5621–5629.

Wicker-Thomas, C., Garrido, D., Bontonou, G., Napal, L., Mazuras, N., Denis, B., Rubin, T., Parvy, J.P., and Montagne, J. (2015). Flexible origin of hydrocarbon/pheromone precursors in Drosophila melanogaster. J. Lipid Res. *56*, 2094–2101.

Wigglesworth, V.B. (1988). The source of lipids and polyphenols for the insect cuticle: the role of fat body, oenocytes and oenocytoids. Tissue Cell *20*, 919–932.

Wisely, G.B., Miller, A.B., Davis, R.G., Thornquest, A.D., Jr., Johnson, R., Spitzer, T., Sefler, A., Shearer, B., Moore, J.T., Miller, A.B., et al. (2002). Hepatocyte nuclear factor 4 is a transcription factor that constitutively binds fatty acids. Structure *10*, 1225–1234.

Yamagata, K., Furuta, H., Oda, N., Kaisaki, P.J., Menzel, S., Cox, N.J., Fajans, S.S., Signorini, S., Stoffel, M., and Bell, G.I. (1996). Mutations in the hepatocyte nuclear factor-4alpha gene in maturity-onset diabetes of the young (MODY1). Nature *384*, 458–460.

Yin, L., Ma, H., Ge, X., Edwards, P.A., and Zhang, Y. (2011). Hepatic hepatocyte nuclear factor 4α is essential for maintaining triglyceride and cholesterol homeostasis. Arterioscler. Thromb. Vasc. Biol. *31*, 328–336.

Yuan, X., Ta, T.C., Lin, M., Evans, J.R., Dong, Y., Bolotin, E., Sherman, M.A., Forman, B.M., and Sladek, F.M. (2009). Identification of an endogenous ligand bound to a native orphan nuclear receptor. PLoS One *4*, e5609.

Zhong, W., Sladek, F.M., and Darnell, J.E. (1993). The expression pattern of a Drosophila homolog to the mouse transcription factor HNF-4 suggests a determinative role in gut formation. EMBO J. *12*, 537–544.

STAR★METHODS

KEY RESOURCES TABLE

REAGENT or RESOURCE	SOURCE	IDENTIFIER
Antibodies		
Affinity-purified guinea pig anti dHNF4 antibody	Palanker et al. (2009)	N/A
Chemicals, Peptides, and Recombinant Proteins		
Methyl 4-hydroxybenzoate sodium salt	Sigma-Aldrich	85265-500G
Oil Red O	Sigma-Aldrich	O0625-25G
7(Z)-tricosene	Cayman Chemical	Cat# 9000313
Tricosane	Sigma-Aldrich	263850
7(Z)-pentacosene	Cayman Chemical	Cat# 9000530
(Z), 11(Z)-heptacosadiene	Cayman Chemical	Cat# 10012567
Critical Commercial Assays		
Hexokinase kit glucose assay	Sigma-Aldrich	GAHK20
Amyloglucosidase	Sigma-Aldrich	A1602-25MG
Triglyceride reagent	Sigma-Aldrich	T2449-10ML
Free glycerol reagent	Sigma-Aldrich	F6428-40ML
Protein reagent	BioRad	Cat# 5000006
SYBR GreenER qPCR SuperMix Universal	ThermoFisher Scientific	Cat# 11762100
Nucleospin RNA kit	Macherey-Nagel	Cat# 740955.50
Superscript Reverse Transcriptase II	ThermoFisher Scientific	Cat# 18064022
Trizol reagent	Invitrogen	Cat# 15596026
TissueLyser II	Qiagen	Cat# 85300
SuperScript VILO Master Mix	ThermoFisher Scientific	Cat# 11755050
Nuclease-free water	ThermoFisher Scientific	Cat# R0581
Experimental Models: Cell Lines		
Primary control and *HNF4α* mutant mouse hepatocytes	Simcox et al. (2017)	N/A
Experimental Models: Organisms/Strains		
D. melanogaster: w $^{-}$; HNF4$^{\Delta 17}$/CyO, twi-Gal4, UAS-GFP	Palanker et al. (2009)	N/A
D. melanogaster: w $^{-}$; HNF4$^{\Delta 33}$/CyO, twi-Gal4, UAS-GFP	Palanker et al. (2009)	N/A
D. melanogaster: w $^{-}$; EP2449/EP2449 (II)	Palanker et al. (2009)	N/A
D. melanogaster: w $^{-}$; KG08976/KG08976 (II)	Palanker et al. (2009)	N/A
D. melanogaster: HNF4$^{\Delta 17}$,PromE-Gal4: w $^{-}$; HNF4$^{\Delta 17}$,P{w[+mC]= Desat1-GAL4.E800} /CyO, twi-Gal4, UAS-GFP	This paper	N/A
D. melanogaster: w $^{-}$; HNF4$^{\Delta 33}$, UAS-dHNF4 w $^{-}$; HNF4$^{\Delta 33}$, P{w[+]=UAS-dHNF4}/CyO, twi-Gal4, UAS-GFP	Palanker et al. (2009)	N/A
D. melanogaster: PromE-Gal4 P{w[+mC]=Desat1-GAL4.E800} (II)	N/A	N/A
D. melanogaster: PromE-Gal4; Tub-Gal80^{ts} P{w[+mC]=Desat1-GAL4.E800}2M, P{w[+mC]=tubP-GAL80[ts]}20	BDSC	RRID: BDSC_65406
D. melanogaster: UAS-mCherry RNAi y[1] sc[*] v[1]; P{y[+t7.7] v[+t1.8]=VALIUM20-mCherry}attP2	BDSC	RRID: BDSC_35785
D. melanogaster: UAS-dHNF4 RNAi y[1] sc[*] v[1]; P{y[+t7.7] v[+t1.8]=TRiP.HMC05862}attP40	BDSC	RRID: BDSC_64988
D. melanogaster: UAS-KAR RNAi y[1] sc[*] v[1]; P{y[+t7.7] v[+t1.8]=TRiP.HMC05887}attP40	BDSC	RRID: BDSC_65013
D. melanogaster: UAS-KAR RNAi (#2) y[1] sc[*] v[1]; P{y[+t7.7] v[+t1.8]=TRiP.GL00567}attP2	BDSC	RRID: BDSC_36607

(*Continued on next page*)

Continued

REAGENT or RESOURCE	SOURCE	IDENTIFIER
D. melanogaster: UAS-ACC RNAi y[1] sc[*] v[1]; P{y[+t7.7] v[+t1.8]=TRiP.HMS01230}attP2	BDSC	RRID: BDSC_34885
D. melanogaster: UAS-FASN^{CG17374} RNAi y[1] sc[*] v[1]; P{y[+t7.7] v[+t1.8]=TRiP.HMS05300}attP40	BDSC	RRID: BDSC_63026
D. melanogaster: UAS-Cpr RNAi y[1] v[1];P{y[+t7.7] v[+t1.8]= TRiP.HMC03369}attP40/CyO	BDSC	RRID: BDSC_51809
D. melanogaster: UAS-Cyp4g1 RNAi *y[1] sc[*] v[1]; P{y[+t7.7] v[+t1.8]=TRiP.HMS01628}attP40*	BDSC	RRID: BDSC_36737
D. melanogaster: UAS-CPT1 RNAi y[1] v[1]; P{y[+t7.7] v[+t1.8]=TRiP.HMS00040}attP2/TM3, Sb[1]	BDSC	RRID: BDSC_34066
D. melanogaster: UAS-CPT2 RNAi y[1] v[1];P{y[+t7.7] v[+t1.8]=TRiP.HMC03474}attP40	BDSC	RRID: BDSC_51900
D. melanogaster: UAS-mtpα RNAi y[1] sc[*] v[1]; P{y[+t7.7] v[+t1.8]=TRiP.HMS00660}attP2	BDSC	RRID: BDSC_32873
D. melanogaster: UAS-scully RNAi y[1] v[1]; P{y[+t7.7] v[+t1.8]=TRiP.HMS02305}attP40	BDSC	RRID: BDSC_41884
w^{1118}	N/A	N/A
Canton-S	N/A	N/A
Oligonucleotides		
See Table S1 for Primer sequences for RT-qPCR	This paper	N/A
Software and Algorithms		
ImageJ	NIH Image	https://imagej.net/ImageJ
QuantStudio® 3 - 96-Well 0.2 mL Block with Data connect	Applied Biosystems/ ThermoFisher Scientific	https://apps.thermofisher.com/apps/dataconnect/
Infinity 3 Lumenera camera and Infinity Analyze software	Lumenera	N/A
Graphpad prism 6 software	Graphpad software	https://www.graphpad.com/scientific-software/prism/
Other		
Dense weave cellulose acetate stopper for fly vials	Genesee Scientific	Cat# 49-101
Fly Polystyrene vials	Genesee Scientific	Cat# 32-110
Invitrogen Countess cell counting chamber slide	ThermoFisher Scientific	Cat# C10228

CONTACT FOR REAGENT AND RESOURCE SHARING

Further information and requests for resources and reagents should be directed to and will be fulfilled by the Lead Contact, Carl Thummel (carl.thummel@genetics.utah.edu).

EXPERIMENTAL MODEL AND SUBJECT DETAILS

Drosophila Strains and Handling

A detailed list of fly strains and genotypes used for these studies is provided in the Key Resources Table. *dHNF4* mutants are trans-heterozygotes for *dHNF4* null alleles (*w^{-}; dHNF4$^{\Delta 17}$/dHNF4$^{\Delta 33}$*), which were generated previously by imprecise excision of *P*-element insertions (*EP2449* and *KG08976*) as described (Palanker et al., 2009). Genetically-matched controls throughout the paper are transheterozygotes for precise excisions of the *EP2449* and *KG08976 P*-elements (*w^{-}; EP2449/KG08976*). For tissue-specific transgene expression, we used the *PromE-Gal4* driver (also known as *P{Desat1-GAL4.E800}*) and the temperature-sensitive *PromE-Gal4, Tub-Gal80^{ts}* driver. *PromE-Gal4* drives expression in larval and adult oenocytes, as well as in the male accessory gland (Billeter et al., 2009; Bousquet et al., 2012). For gene silencing, we used RNAi transgenes from the Transgenic RNAi Project (TRiP, https://fgr.hms.harvard.edu/fly-in-vivo-rnai), available through the Bloomington Drosophila Stock Center (BDSC). Tissue-specific expression of *UAS-mCherry RNAi* was used as control. Fly strains were routinely kept at room temperature on a standard diet composed of yeast, cornmeal, corn syrup, and malt. For experiments, parents were crossed in six ounce square bottom plastic bottles (Genesee Scientific Cat# 38354) containing the 0% sugar diet (recipe below) at 25°C unless otherwise stated. Progeny were collected at emergence and transferred to *Drosophila* polystyrene vials (Genesee Scientific Cat# 32-110) at a density of

5-10 animals/vial. Flies were kept at different temperatures for different experiments as described in the figure legends or as stated below. Males were used for all experiments, except for Figures S3C and S7A–S7D.

Fly Diets

0% sugar diet: For 1L: 80g active dry yeast, 10g agar, 0.5g $MgSO_4$, 0.5g $CaCl_2$. 15% sugar diet: For 1L: 80g active dry yeast, 10g agar, 50g sucrose, 100g glucose, 0.5g $MgSO_4$, 0.5g $CaCl_2$. Ingredients were mixed with water and brought to boil in a microwave oven. After cooling, 4 mL of 99% propionic acid and 5.2 g methyl 4-hydroxybenzoate sodium salt (Sigma-Aldrich Cat# 85265-500G) was added to the mixture and the solution was poured into vials or bottles.

HNF4α Mutant Mouse Hepatocytes

All mouse procedures were approved by the Institutional Animal Care and Use Committee (IACUC) at the University of Utah. Animals were maintained in 12 hr light/12 hr dark cycles at 22°C–24°C and given constant access to water and Teklad global soy protein-free diet (Cat# 2920x-030917M). Food was withdrawn on the day of experimentation. *HNF4α*$^{F/F}$ mice were bred to *C57BL/6* mice for five generations before crossing to homozygosity (Hayhurst et al., 2001). At 12 weeks of age, male *HNF4α*$^{F/F}$ mice received an intravenous injection of 400 μL of adeno-associated virus 8 (AAV8) encoding either eGFP (*AAV8-TBG-eGFP*) or Cre recombinase (*AAV8-TBG-Cre*) regulated by thyroid hormone binding globin (TBG) to drive hepatocyte specific expression (titer 10^{12} genome copies/mL) (Hayashi et al., 1993; Simcox et al., 2017). One week after virus administration, the mice were fasted for 5 hours starting at 10am. At 3pm the mice were anesthetized using 5% isoflurane until unresponsive to pedal reflex test and then sacrificed by cervical dislocation. Tissues were harvested and flash frozen in liquid nitrogen for later processing.

METHOD DETAILS

Lifespan Studies on 0% and 15% Sugar Diets

Animals were collected at adult emergence (eclosion) and transferred to polystyrene vials (Genesee Scientific Cat# 32-110) containing fly food at a density of 5-10 males per vial at 25°C unless otherwise stated. Vials were closed with a dense weave cellulose acetate stopper (Flug; Genesee Scientific Cat# 49-101) to reduce water evaporation from the food. Animals were transferred weekly to vials containing fresh media and lethality was assayed every 1-2 days. Experiments were repeated two to three times and a representative experiment was selected for the figures.

Studies on Diets with Increased Humidity

Animals were collected at emergence and transferred to polystyrene vials (Genesee Scientific Cat# 32-110) containing fly food at a density of 5-10 males per vial. To increase humidity, a dense weave cellulose acetate stopper (Genesee scientific Cat# 49-101) was saturated with water and covered with parafilm. The lifespan and metabolite studies in increased humidity shown in Figures 7F, 7G, S6C, S6D, and S6E were performed at room temperature (approximately 21°C) to avoid excessive condensation in the vials. For the lifespan and metabolite studies performed with the *PromE>, tub-Gal80*^{ts} driver in increased humidity (Figures 7D and 7E), animals were raised at room temperature during development and transferred to 25°C (instead of 29°C) to avoid excessive condensation in the vials while allowing *PromE-Gal4* driven expression of UAS-transgenes. Non-humid controls for these experiments were kept at room temperature or 25°C depending on the experiment. Experiments were repeated two to three times, pooled data from these experiments is depicted in Figures 7F, S6C, and S6D, while a representative experiment is presented in Figure 7D.

Starvation

Polystyrene vials (Genesee Scientific Cat# 32-110) were half filled with water and a dense weave cellulose acetate stopper (Genesee Scientific Cat# 49-101) was pushed to the bottom of the vial allowing saturation of this artificial substrate with water. Excess water was discarded and newly-emerged flies were transferred to these vials at a density of 5-10 males per vial. Vials were sealed with a second dense weave cellulose acetate stopper to reduce water evaporation. For most starvation experiments, animals were kept at room temperature (approximately 21°C) and transferred to a new starvation vial twice a week. Some starvation experiments were conducted at 29°C (Figure 5D). In this case, animals were transferred daily to fresh starvation vials and collected at 3-5 days after emergence for Oil Red O stains. We noticed that despite daily transfers to fresh hydrated vials, the lifespan of starved animals at 29°C is dramatically reduced compared to animals kept at room temperature.

Dry Starvation

For starvation in dry condition (Figures 6B–6D, S7B, and S7C), adults were collected at emergence and kept in standard (hydrated) starvation conditions at a density of 5-10 animals/vial for three days, to provide time for hydrocarbon synthesis (Figures 5B, 6A, and S5A). Animals were then transferred to empty polystyrene vials sealed with a dense weave cellulose acetate stopper and kept at room temperature. Lethality was scored hourly for 10 hours. Experiments were conducted at least three times. Pooled data from these experiments are shown in the figures.

Fly Water Content Determination

Animals were collected at emergence and kept in standard (hydrated) starvation conditions at a density of 5-10 males/vial for three days before being anesthetized using CO_2. Pools of ten animals were weighed using a precision scale (T=0 hour). Animals were then exposed to dry conditions by transferring them to empty polystyrene vials sealed with a dense weave cellulose acetate stopper at room temperature. After 2.5 hrs of dry starvation, animals were anesthetized and weighed with a precision scale (T=2.5 hours). Animals were then transferred to humid starvation conditions and weighed after a 2 hr recovery period (T=4.5 hours) before being rapidly killed by exposing them to -20°C. The following day, carcasses were exposed to the open air and left to dry for a period of 4 days, after which they were weighed in pools of 10 to determine their dry weight. Fly water content (in percentage of body weight) at each time point was calculated using the formula: Water content = $((Weight_T - \text{average dry weight})/Weight_T) \times 100$. The dry weight was assumed to be constant between T=0 and T=4.5 hours.

Metabolite Assays

Whole body glycogen and glucose levels were determined using a hexokinase assay kit (Sigma GAHK20) and amyloglucosidase (Sigma A1602-25MG). Whole body triglyceride levels were determined using the triglyceride reagent (Sigma T2449-10ML) and the free glycerol reagent (Sigma F6428-40ML). Metabolite assays were performed as described with minor modifications (Tennessen et al., 2014). Unless otherwise stated, glucose, glycogen and triglyceride levels were normalized to protein to compensate for variations in sample homogenization and/or animal size. Protein levels were determined using a Bradford assay (BioRad Cat# 5000006). At least four replicates of 4-5 males were used for each sample in metabolite assays. Independent experiments were performed 2-3 times. Figures illustrate a representative experiment (Figures 1B, 1C, 4C, 7C, 7E, 7G, S6B, and S6E) or pooled data from all experiments (Figures 2A, 2B, 2D, S1B–S1D, and S2C). For triglyceride measurements in hemolymph (Figure S2C), the abdomens of five males were opened in 120 μL PBS. Animals were gently shaken to facilitate the diffusion of hemolymph as well as free-floating larval adipose cells in PBS. Carcasses were discarded and the remaining solution was homogenized and used for triglyceride assays. Triglyceride levels were normalized to the number of animals rather than protein for this experiment.

Larval Adipose Cell Counts

An abdomen from a single male was dissected in 10μL PBS. The gut was removed and the carcass was gently shaken to allow the larval adipose cells to disperse in PBS. The carcass was discarded and the larval adipose cells were harvested with a pipet and deposited into an Invitrogen Countess cell counting chamber slide (ThermoFisher Cat# C10228). Cell counting slides were placed upside-down and observed by bright field microscopy using a Zeiss Axioskop2 Plus microscope. Pictures were taken to cover the entire slide and thus capture all the larval adipose cells collected from a single fly. The cumulative surface of larval adipose cells (in pixels) was determined using ImageJ software (https://imagej.nih.gov/ij/download.html). A macro was created to automate the process. Cumulative cell surface was determined rather than larval adipose cell number because these cells can form aggregates that impair automated counting. Six to twelve animals were analyzed per condition. Each dot in Figure S2B represents a single animal.

GC/MS Hydrocarbon Analysis

Males were collected at emergence, or after being starved or fed a 0% sugar diet for 3 days. Five samples of 20 animals were collected per condition. Sample preparation and gas chromatography/mass spectrometry (GC/MS) analysis were performed by the Metabolomics Core Research Facility at the University of Utah School of Medicine. The identity of some hydrocarbon species was confirmed by comparison with purified standards (7(Z)-tricosene (Cayman Chemical Cat# 9000313), tricosane (Sigma-Aldrich Cat# 263850), 7(Z)-pentacosene (Cayman Cat# 9000530) and 7(Z), 11(Z)-heptacosadiene (Cayman Chemical Cat# 10012567). The identity of other hydrocarbon species detected in the samples was determined by their ionization mass.

Oil Red O Stains

Oil red O stains were performed as described with minor modifications (Tennessen et al., 2014). Briefly, abdominal cuticles (containing adipose tissue and oenocytes) of 10 animals were dissected in PBS and fixed in 4% formaldehyde for one hour at room temperature. They were washed twice in PBS and twice in propylene glycol before being incubated for one hour at 60°C in Oil red O diluted in propylene glycol. Cuticles were then washed twice in propylene glycol and twice in PBS. Fat body and oenocytes were dissected by gently scraping the inner side of the abdominal cuticle with forceps in a drop of glycerol on a microscopy slide. A coverslip was then deposited on top of the dissected tissues before observation by bright field microscopy. Pictures were taken with a Zeiss Axioskop Plus microscope equipped with an Infinity 3 Lumenera camera and the Infinity Analyze software. Independent Oil red O stains were performed two to three times on sets of 10 cuticles and a representative image is shown in each figure. For larval adipose cells, male abdomens were dissected in PBS, the gut was removed and the carcass was shaken gently to allow larval adipose cells to disperse in PBS. Larval adipose cells were then collected by pipetting and transferred to a 1.5mL Eppendorf tube. Larval adipose cells were washed and stained with Oil red O as described except that they were collected by centrifugation between each step.

Immunostaining to Detect dHNF4 Protein

Affinity-purified guinea pig anti-dHNF4 antibodies were used for immunofluorescence studies as described (Palanker et al., 2009). Abdominal cuticles were dissected in cold PBS, fixed in 4% formaldehyde for 30 min at room temperature, and washed three times

for 10 min each in PBS, 0.2% Triton-X100. Samples were blocked using 5% normal goat serum for 1.5–2 hours at room temperature and incubated with primary antibodies for a minimum of 12 hours at 4°C. They were washed and incubated with secondary antibody at room temperature (approximately 21°C) for two hours. Abdominal cuticles were then mounted in glycerol. Images were acquired using a Zeiss Axioskop2 Plus microscope equipped with a X-Cite 120 LED*Boost* from Excelitas Technologies.

RT-qPCR

Real Time-qPCR (RT-qPCR) experiments were conducted with an Applied Biosystem Quantstudio 3 device. SYBR GreenER qPCR SuperMix Universal (ThermoFisher Scientific Cat# 11762100) was used for RT-qPCR reactions. ROX was diluted ten times and 0.1 μL was added to the mix for a final reaction volume of 20 μL. Fold inductions in transcript level were determined using the ΔΔCt method. For the *Drosophila* samples, transcript levels were normalized to *rp49*. For the mouse samples, transcript levels were normalized to *Rpl13*. RT-qPCR experiments were conducted on 4 to 5 independent *Drosophila* cDNA samples per condition, and 6 independent mouse hepatocyte cDNA samples per condition. The figures represent the combined data from all samples. A list of primers used in our RT-qPCR experiments is available in Table S1. We used primers for RT-qPCR experiments after confirming an efficiency between 90 and 110%.

cDNA Synthesis from *Drosophila* Tissues

RNA was extracted from samples of 5 to 10 males using the Nucleospin RNA kit from Macherey-Nagel (Cat# 740955.50). Reverse transcription was performed on 0.25-1 μg RNA using the Superscript Reverse Transcriptase II from ThermoFisher Scientific (Cat# 18064022) and oligo(dT) primers. cDNA was used as a template for qRT-PCR as described above.

cDNA Synthesis from Mouse Hepatocytes

RNA was isolated from the left lobe of the liver using Trizol reagent (Invitrogen Cat# 15596026). The only deviation from the manufacturers protocol was an extra centrifugation at 7,500xg to remove excess lipids directly after homogenization with the TissueLyser II (Qiagen Cat# 85300). SuperScript VILO Master Mix (Thermofisher Cat# 11755050) was used for reverse transcription with a starting concentration of 1 μg RNA for each sample, after which cDNA samples were diluted 1:10 with nuclease-free water (Thermofisher Cat# R0581). cDNA was used as a template for qRT-PCR as described above.

Information Related to Experimental Design

Blinding was not used in the course of our study. No data or subjects were excluded from our analyses.

QUANTIFICATION AND STATISTICAL ANALYSIS

Graphical Representation and Statistical Analysis of the Data

Graphical representation and statistical analysis of the data were performed using GraphPad Prism 6 software (www.graphpad.com).

For lifespan studies, data is presented as Kaplan-Meier survival plots. Short black vertical lines on the plot indicate when animals were removed from the experiment, for example when flies escaped during their transfer to a new vial (Figures 7A and 7B). The number of animals used in lifespan experiments and the median lifespan in each condition are indicated in the figure legends. A Log-Rank (Mantel-Cox) test was used for statistical comparison of survival plots. The p-value is indicated in the figure legends when the difference is statistically significant.

For glucose, glycogen and triglyceride assays scored at a single time point, data are represented by box and whiskers plots. Data are represented as XY graphs when metabolite levels were scored at multiple time points (Figures 2A, 2B, 2D, S1B–S1D, and 4C). For box and whiskers plots, the box extends from the 25th to 75th percentiles, the line represents the median, and the whiskers represent minimum and maximum values. For XY graphs, the dots represent mean values and the error bars represent standard deviation. We used a Mann-Whitney test for pairwise comparisons with both types of data/representations. Asterisks illustrate statistically significant differences between conditions. ****$p<0.0001$; $0.0001<$***$p<0.001$; $0.001<$**$p<0.01$; $0.01<$*$p<0.05$

To analyze cumulative larval adipose cell surfaces after emergence (Figure S2B), the data is presented as grouped individual values. Each dot represents the cumulative larval adipose cell surface from a single male. The black horizontal line in the dot plot represents the mean, and the black error bars represent the standard deviation. We used a Mann-Whitney test for pairwise comparisons. Asterisks illustrate statistically significant differences between controls and *dHNF4* mutants at a given timepoint: ****$p<0.0001$.

For the analysis of fly water content upon dry starvation (Figure 6E), dots represent average water content at each time point ($11<n<13$), and the error bars represent the standard deviation. We used a Mann-Whitney test for pairwise comparisons. Asterisks illustrate statistically significant differences between controls and *dHNF4* mutants: ****$p<0.0001$. Experiments were repeated three times, one representative experiment is shown in the figure.

For transcript analysis by RT-qPCR (Figures 5B, 6G, and S4C), the data is presented as histograms. Each bar represents the mean and the error bars represent the standard deviation. We used a Mann-Whitney test for pairwise comparisons. Asterisks illustrate statistically significant differences between controls and *dHNF4* mutant *Drosophila*, or between controls and *HNF4α* mutant mouse hepatocytes: $0.001<$**$p<0.01$; $0.01<$*$p<0.05$.

For hydrocarbon levels (Figures 6A and S5A), the data is presented as interleaved box and whiskers plots. The box extends from the 25th to 75th percentile, the line represents the median, and whiskers represent minimum and maximum values. For pairwise comparisons between controls and *dHNF4* mutants at each time point (Day 0, Day 3 starv. and Day 3 0% sugar diet) we performed multiple t-tests. We did not assume consistent standard deviations, and set a desired false discovery rate (Q) value of 1.000%. A single asterisk represents a p-value below the cutoff ($p<0.01$).

No specific method was used to determine whether the data met the assumptions of the statistical approach.